Electric Power Systems Research 244 (2025) 111594

Contents lists available at ScienceDirect

Electric Power Systems Research

journal homepage: www.elsevier.com/locate/epsr

An adaptive protection scheme for an inverter-dominated grid considering Momentary Cessation

Emad Eldeen Omran [a], Feras Alasali [b], Naser El-Naily [c], Hassen Loukil [d], Abdelaziz Salah Saidi [e], William Holderbaum [f,*], Azza A. ElDesouky [g]

[a] Department of Electrical Engineering, Faculty of Engineering, Suez Canal University, Ismailia 41522, Egypt
[b] Department of Electrical Engineering, Faculty of Engineering, The Hashemite University, Zarqa 13133, Jordan
[c] Department of Electrical Engineering, College of Electrical and Electronics Technology, Benghazi 5213, Libya
[d] Department of Electrical Engineering, College of Engineering, King Khalid University, Abha 61421, Saudi Arabia
[e] Grid Studies Department, National Grid SA, Riyadh 13341, Saudi Arabia
[f] School of Science, Engineering and Environment, University of Salford, Salford, UK
[g] Department of Electrical Engineering, Faculty of Engineering, Port Said University, Port Fouad 42526, Egypt

ARTICLE INFO

Keywords:
Inverter-based renewable energy resources
Overcurrent Relay
Momentary Cessation mode
Islanding

ABSTRACT

The increased penetration of Inverter-Based Renewable Energy Resources (IBRERs) enhances the power system's reliability and stability. However, it has a considerable influence on Overcurrent Relays (OCRs) protection systems due to the higher amplitude of short circuit current and bidirectional flow. Furthermore, the Momentary Cessation (MC) mode of IBRERs can have an impact on power system protection since it temporarily ceases significant amounts of IBRER generation. This paper addresses the impact of the IBRERs 's MC on the protection distribution system. A comprehensive four-case study on the CIGRE 14-bus distribution network is presented to investigate the challenges of miscoordination and false tripping caused by increased IBRER penetration. This study introduces an adaptive protection scheme that combines current-based and voltage-based logic to enhance fault detection and relay response. The proposed approach ensures rapid, accurate, and adaptive protection under diverse fault scenarios, thereby improving system reliability and operational resilience. Furthermore, different IBRER working modes and OCR schemes are suggested to be tested and carried out using a simulation built on MATLAB/ ETAP software. The results of the study demonstrate the importance of this research as a crucial reference for future research by high levels of renewable energy penetration.

1. Introduction

Inverter-Based Renewable Energy Resources (IBRERs) have gained popularity recently as a means of enhancing Distribution Networks (DNs) due to their various benefits, which include lower fuel prices, carbon emissions, and the capacity to minimize power losses and enhance Power Quality (PQ) service on distribution lines [1–4]. However, increasing IBRERs penetration always results in not only an increase in short-circuit current but also an obvious change in relaying fault current, either increasing or decreasing in magnitude or changing in direction depending on the IBRERs connection point relative to the relaying points. Since the Overcurrent Relay (OCR) function is dependent only on the fault current magnitude detected at the relaying sites, the IBRER connection has a significant impact on its performance and coordination. Moreover, when a major disruption occurs and considerable variations in the system voltage or frequency are detected, the IBRER activation is briefly halted, known as Momentary Cessation (MC). The IBRERs operating in the MC mode's voltage range ($V < 0.50$ p.u and $1.10 < V < 1.20$ p.u) deliver neither active nor reactive power to the power system. The MC function originally had the goal of reducing the IBRER contribution to the fault current, thereby protecting the distribution system. However, because the IBRER contribution to power systems has expanded significantly, distribution systems can now be severely impacted by MC operation. The MC allows for the immediate restoration of IBRER when the system voltage and frequency return to acceptable levels. If the transient disturbance is removed before the ride-through minimum time (≥ 1 s), the IBRER can immediately restore power to the remainder of the grid. High photovoltaic)PV(penetration's

* Corresponding author.
E-mail address: w.holderbaum@salford.ac.uk (W. Holderbaum).

https://doi.org/10.1016/j.epsr.2025.111594
Received 5 October 2024; Received in revised form 31 January 2025; Accepted 3 March 2025
Available online 6 March 2025

effects on transient and steady-state stabilities had been examined [5]. The fluctuation in bus voltage magnitude as a function of PV penetration level was investigated to evaluate steady-state stability, and the effects of PV penetration on transient stability were also investigated using simulation studies. The effects of synchronous, asynchronous, and Distributed Generator (DG) units on transient and voltage stability were examined using a time-domain simulation [6]. Meanwhile, an IBRER model with MC capacity has been presented for reliability investigations [7,8]. However, a limited number of researchers have investigated how MC affects power system transient stability. The stability margin was calculated using a single machine equivalent technique, which addressed the direct influence of the MC recovery ramp rate on the power system's transient stability [9]. The key MC recovery ramp rate for a particular system was also introduced in this research, and it might be a useful index when planning an IBRERs installation. In [10], the authors examined how voltage fluctuation caused by faults in transmission and DNs affects DN voltage delay recovery and MC/trip functioning of smart IBRERs. The study proposed a monitoring and management strategy that integrates information from synchro phasors and phasor data concentrators to improve smart inverter deployment, dynamic functions, and decoupling between distribution and transmission operations. The crucial MC voltage was defined in [11] to ensure power system stability and the geographical reliance of IBRERs was estimated on the power system. In the Korean electricity system, the essential MC voltage's viability and efficacy were shown. To confirm the results, transient stability evaluation was employed. In [12], it was covered how the MC of IBRERs affected distribution system protection. The study used a modified IEEE 123 node system to simulate the effects of MC on the fault current and the operation of time overcurrent elements. While some research has explored the impact of IBRERs on the power grid performance, limited studies have specifically investigated how PV control strategies and MC influence OCR behavior, especially under varying fault conditions. This is a critical gap, as the PV control can significantly affect fault current dynamics, and understanding its role is essential for improving relay coordination. As a result, there is a need to investigate and develop protection strategies to address the high penetration of IBRERs, particularly PV systems, and the concerns about the effects of MC on OCR coordination.

In the presence of on-load tap changers (OLTCs), a reliable protection coordination approach using Directional Overcurrent Relays (DOCRs) was presented [13]. Single DOCR settings were made available by the robust protection coordination approach, and they would apply to all N − 1 scenarios that were formed following the outage of a generator, transformer, or wire. The most efficient protection coordination for Micro-Grids (MGs) made up of RERs and Energy Storage Systems (ESS) that are both islanded and grid-connected was explained [14]. The recommended operation approach reduced the operation cost of DGs and ESSs as well as the load-shedding cost of the islanded MG by using AC power flow equations, system operating limits, and DG and ESS equations as issue constraints. In [15], a user-defined OCR characteristic was used to attain the minimal operating duration while meeting protective coordination criteria, hence mitigating the possible consequences of DGs on the DN. This paper proposed a hybrid optimization technique based on linear programming and metaheuristics that may find the best solution while using less computational time. In [16] the authors employed resilient and adaptive coordination techniques to determine the best directional OCR configuration, get an acceptable degree of PQ and enable selective activation of DOCRs under network topology change circumstances. Additionally, taking into account the significance of voltage dip, an objective function with three basic components was utilized. An approach based on the adaptability of IBRERs controls was presented [17] where proper IBRERs current magnitude and angle settings could recover fault current levels and DOCR operation times. The IBRERs parameters were formulated as a non-linear optimization challenge to keep each DOCR operation period within the restricted range after IBRERs integration. Furthermore, the settings of IBRERs were optimized in the presence of dispersed synchronous generators. The authors of [18] investigated the sympathetic trip in the presence of synchronous DGs. Equations for the role of DGs and the upstream network in supplying short circuit current were derived. The impact of various characteristics on the probability of experiencing a sympathetic trip was also investigated. Furthermore, an innovative and quick approach was proposed for overcoming the sympathetic trip of synchronous DGs. In [19], the optimal coordination of directional OC protections was discussed, considering the possibility of different system configurations and the impact of grouping situations. The optimization was designed for certain topologies to determine the best Bundle of Protection Settings (BPS) for each subgroup. The amount of BPS was regulated by the relay's configuration groups. A slowness index (σ) was generated for each subgroup solution in comparison to the best reference topology. A study examined how IBRERs affect the performance of Sequence-Based Directional Relaying Systems (SBDRS) [20]. CIGRE-14 bus system with IBRERs and comprehensive modelling of the inverter control method (with and without grid codes) and SBDRS had been conducted in the PSCAD environment. The implications of the standard, such as MC capabilities, on smart inverters were discussed [21].

1.1. Contributions

Considering the reviews of earlier research, none of these studies explored the effect of an MC's inverter operating mode on the performance and coordination of OCR protection systems. In this work, the focus is placed on investigating the impact of the MC mode on OC protection schemes, particularly how this mode affects the coordination and detection capabilities of protection relays in different fault scenarios. Through comprehensive simulations using the CIGRE 14-bus DN, this study aims to explore the challenges associated with fault detection and relay coordination when RERs, especially solar PV systems, enter the MC mode. By addressing this research gap, this paper seeks to contribute to a deeper understanding of the influence of MC on the effectiveness of OC protection in evolving power systems with high penetration of RERs. Given this, the main motivations of the paper are:

- Detailed investigation into the effect of MC on OCR protection and understanding of the behavior of protection relays under these unique conditions, which is crucial for adapting existing protection strategies.
- Presenting four cases studied through simulations conducted using the CIGRE DN model in MATLAB/ETAP which provides important insights into how MC can unexpectedly support protection coordination in specific configurations, despite reducing overall fault current levels.
- Identifying challenges in island mode operation that indicate an inability to maintain selective fault isolation and renders traditional OC protection schemes ineffective.
- By providing empirical evidence on the effects of MC mode on OC protection coordination, the study serves as a crucial reference for future research and development of protection schemes in modern power systems, helping to address the challenges posed by high levels of renewable energy penetration.
- Development of an adaptive OCR protection scheme: The proposed protection scheme introduces a new approach that integrates current-based and voltage-based protection logic for MC mode. By dynamically switching between the standard inverse OCR and voltage-controlled MC components, the scheme ensures optimal response under diverse fault scenarios, enhancing system adaptability, speed, and reliability.

1.2. Outline of paper

The remainder of the work is structured as follows: OCRs coordination challenges for a power network with IBRERs is described in Section

2, including the OCRs coordination for networks with and without the MC. Section 3 presented the simulation results for the four cases. In Section 4, the conclusion is finally concluded.

2. OCRs coordination challenges for a power network with IBRERs

OCR is one of the fundamental elements in electrical protection systems, designed to detect instances of excessive current flow that may occur in the network due to electrical faults such as short circuits or abnormal load increases. The principle of OC protection is based on ensuring that the current within the system remains within predetermined limits, and when these limits are exceeded, protection devices such as relays are activated to disconnect the affected part of the network. This action prevents the fault from spreading and protects electrical equipment from potential damage.

2.1. Power network OCRS coordination

The coordination of OC protection is achieved by setting appropriate values for the relay's pickup current and operating time, ensuring a selective disconnection sequence in the event of faults. This coordination process aims to guarantee that the relay closest to the fault location operates first to isolate the affected area, thereby maintaining power supply continuity to other parts of the network. The coordination is realized by adjusting settings such as the Time Multiplier Setting (TMS) and the pickup current, enabling a time-sequenced operation that corresponds to the relay's position relative to the power source. Fig. 1(a) represents a section of the primary network focusing on the detailed coordination process within this specific part of the network. In this network, R4 is configured as the backup relay, while R3 or R10 functions as primary relays for their respective outgoing feeders. The TMS of R4 is adjusted to ensure its operation occurs after R3 or R10, thereby providing sufficient time for either R3 or R10 to clear any downstream faults. This selective coordination is essential, as a Coordination Time Interval (CTI) of 0.3 to 0.4 s (S) is maintained between R4 and the primary relays (R3 or R10), ensuring that R4 only activates if the primary relay fails to isolate the fault. This selective tripping mechanism not only minimizes unnecessary disruptions but also optimizes system reliability. By prioritizing R3 with a longer time setting, effective protection is established ensuring R4 serves as a robust backup relay that intervenes only, when necessary, thereby achieving precise fault discrimination and enhancing overall network protection efficiency. This detailed setup exemplifies the fundamental principles of relay coordination within protection systems.

Fig. 1(b) illustrates a radial network with four buses labeled B8, B9, B10, and B11, each protected by OCR (R3, R2 and R1), respectively. The diagram highlights the process of coordination between primary and backup protection, demonstrating how fault current varies with distance from the relay's position along the cable. Achieving proper coordination ensures that the primary and backup protection systems operate selectively, preventing any overlap or interference between relay operations, thereby maintaining the required reliability and selectivity of the protection scheme. To ensure effective coordination, it is essential to determine the maximum fault current that each relay can detect within its zone of protection. This is achieved by considering the highest fault current observed in the zone, typically occurring near the relay at the beginning of the cable segment, where a three-phase fault close-in results in the highest fault current. This setup excludes the impedance of the cable, ensuring the relay can respond correctly to the highest possible fault current. This approach not only guarantees that the coordination between primary and backup protection is accurately established but also helps in designing circuit breakers capable of handling the maximum short-circuit current in that specific location. Additionally, for the minimum fault current, a two-phase fault (LL)is simulated at the farthest end of the cable segment, beyond relay R1. This situation typically results in the lowest short-circuit current because of the added impedance from the cable length. This helps in establishing the minimum sensitivity levels required for the relays to detect and isolate faults occurring at the end of the radial network.

Furthermore, Fig. 1(b) also shows how the CTI is maintained, especially under the condition of maximum fault current near the start of the cable. This interval is logarithmic, based on the inverse-time characteristic equation of the OC protection scheme, Eq. (1), ensuring that the relays operate with optimal coordination over the varying fault current magnitudes along the radial line [22].

$$t_r = \left[\frac{A}{\left(\frac{I_f}{I_p}\right)^B - 1}\right] TMS \tag{1}$$

where t_r is the operational time, I_f and I_p: The fault and pickup currents, respectively. The constants A and B are determined based on established OCR standards such as IEEE and IEC [22–24]. The specific characteristic equation governing the relay's response varies depending on the

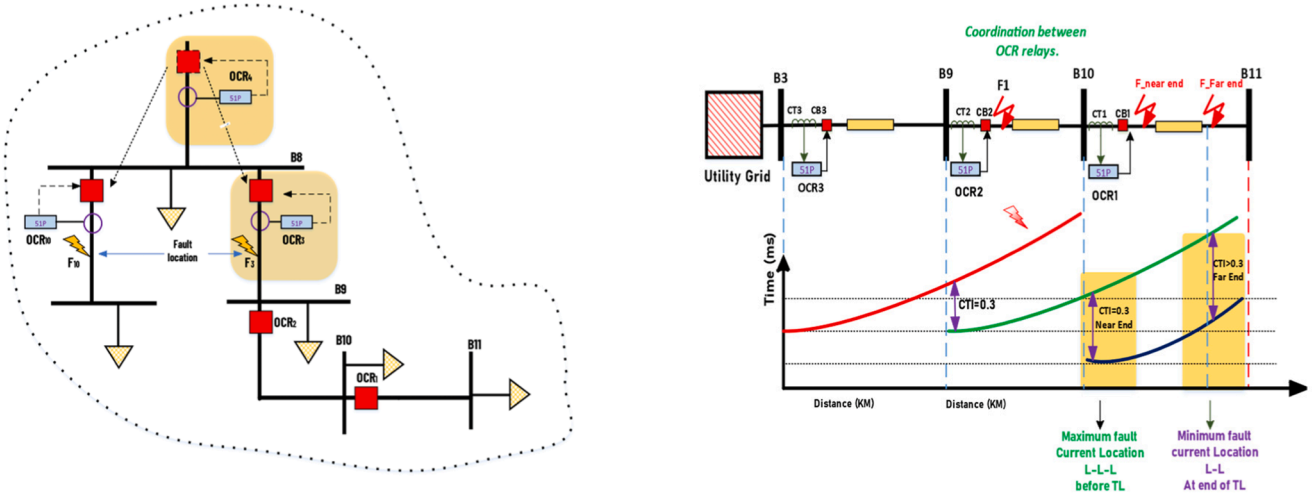

a. Incomer and outgoing b. Radial coordination

Fig. 1. Coordination between OCR ensuring proper fault isolation and system protection.

manufacturer and type of OCR utilized. In this research, a numerical OCR that follows the industry-standard IEC specifications is utilized, with A and B values set at 0.14 and 0.02, respectively, as defined in the relay's operating equation. Fig. 2(a) illustrates the OCR characteristic curves, showing the relationship between multiples of current up to 20 times the rated current and the trip time, while Fig. 2(b) presents a 3D representation of varying TMS values.

2.2. The impact of IBRERs on the protection system

Increasing IBRER penetration leads to increased short-circuit current and noticeable changes in the fault current of the relay via raising or decreasing in magnitude or variation in direction following the IBRER connection point's distance from the relaying locations. The OCR operation relies solely on the quantity of fault current at relay locations, making the IBRER connection crucial [23]. Having an impact on its performance and coordination, MC is a common issue that occurs in power systems particularly those that integrate RERs such as solar panels and wind turbines. The MC mode is a protective operating state in which the inverter temporarily halts power injection into the grid while remaining connected to it. This mode is triggered when grid voltage falls outside the acceptable operating range for mandatory operation typically below 0.5 p.u or above 1.1 p.u. While the inverter stops delivering both active and reactive power during this period, it remains electrically connected to the grid. As soon as the grid voltage recovers and returns to a safer range, the inverter can quickly resume its normal operations without requiring a full reconnection process. This fast resumption capability is crucial in maintaining grid resilience, as it reduces downtime and ensures that the inverter can continue contributing power as soon as conditions normalize. The output characteristics of IBRERs with MC capability are shown in Fig. 3. The goal of this mode is to safeguard both the inverter and the grid by minimizing the contribution of RER systems to fault currents during significant disturbances.

The IBRER systems operate in different modes depending on the transient voltage conditions. Each mode is characterized by specific voltage ranges and behaviors, ensuring the stability and reliability of the power system under varying conditions [25,26] as shown in Fig. 4. The Continuous Operation (CO) mode operates within the voltage range of $0.88 \leq V_{pu} \leq 1.1$ which represents normal operating conditions. In this mode, IBRER s exchange both active and reactive current with the power system, maintaining synchronization without tripping or ceasing to energize. The control strategies in this mode include power factor

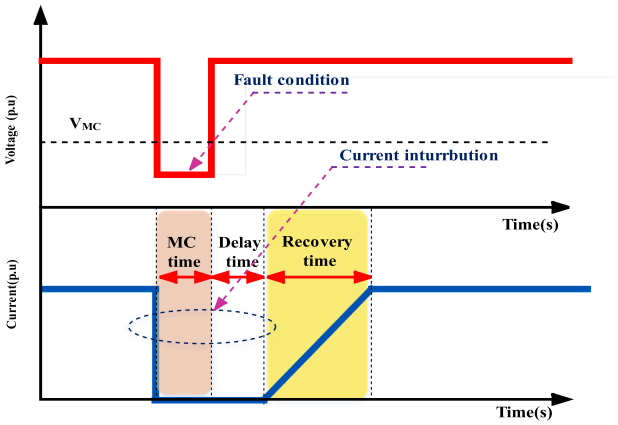

Fig. 3. The characteristic of power output of IBRERs by MC mode [9].

control, voltage control, or reactive power control. The Mandatory Operation (MO) mode is activated under abnormal voltage conditions in the range $0.5 \leq V_{pu} \leq 0.88$ During MO mode, IBRERs continue to operate synchronously, supplying current to the grid within the converter's maximum current limit. This mode ensures grid stability during moderate voltage disturbances. The MC mode comes into effect during severe voltage deviations, specifically $V_{pu} < 0.5$ *or* $1.1 < V_{pu} \leq 1.20$. In MC mode, IBRERs temporarily cease to energize the grid, providing neither active nor reactive power. The original purpose of this mode is to minimize fault current contributions and protect the distribution system. However, with the increasing penetration of IBRERs, this mode can adversely affect system stability and conventional generators by significantly reducing the electrical power supply during transient states [25, 26].

2.3. The short circuit calculation standards in the presence of IBRERs

Fig. 5 presents the equivalent circuit diagram of the IBRERs, where the current source, I_{IBRER} is controlled at point of common coupling (PCC) by the positive sequence voltage, V^{+}_{PCC}, as $I_{IBRER} = f(V^{+}_{PCC})$, the fault current magnitude in IBRERs is influenced by the intermittent RERs and the variation of positive sequence voltage at the PCC (V^{+}_{PCC}) and based on behavior a control function, f. During fault conditions, PV plants operate under different control strategies [23], which can lead to

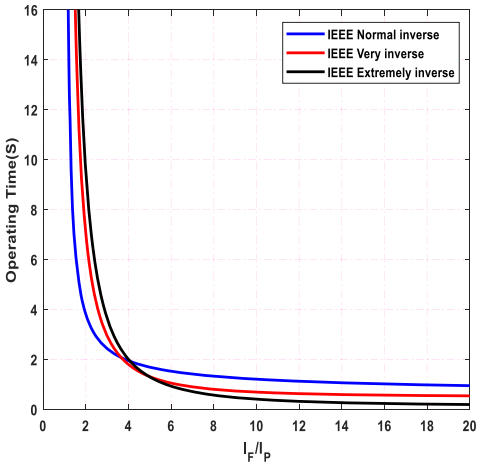

a. OCR curves showing the trip time against current multiples up to 20 times the rated current.

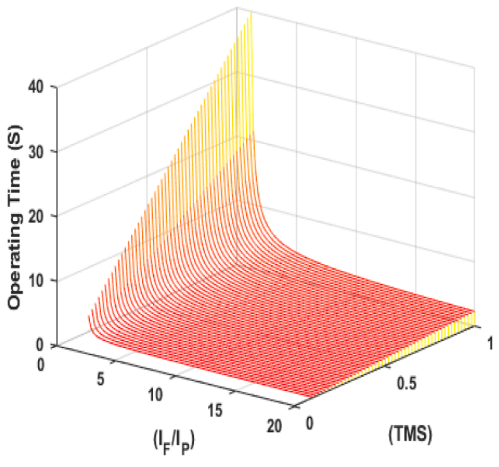

b. 3D representation illustrating the effect of varying TMS values.

Fig. 2. OCR curve illustrating the time-current characteristic.

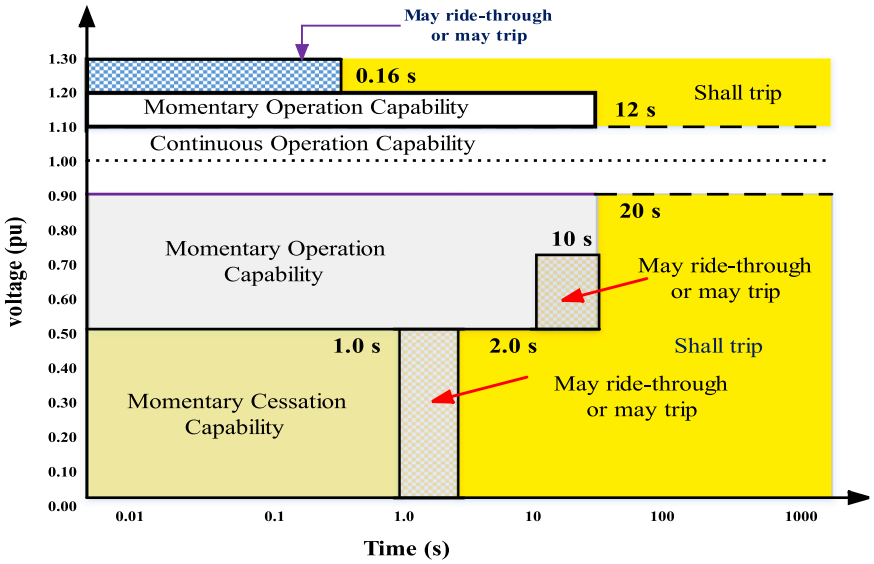

Fig. 4. IBRER response to voltage and voltage ride-through requirements.

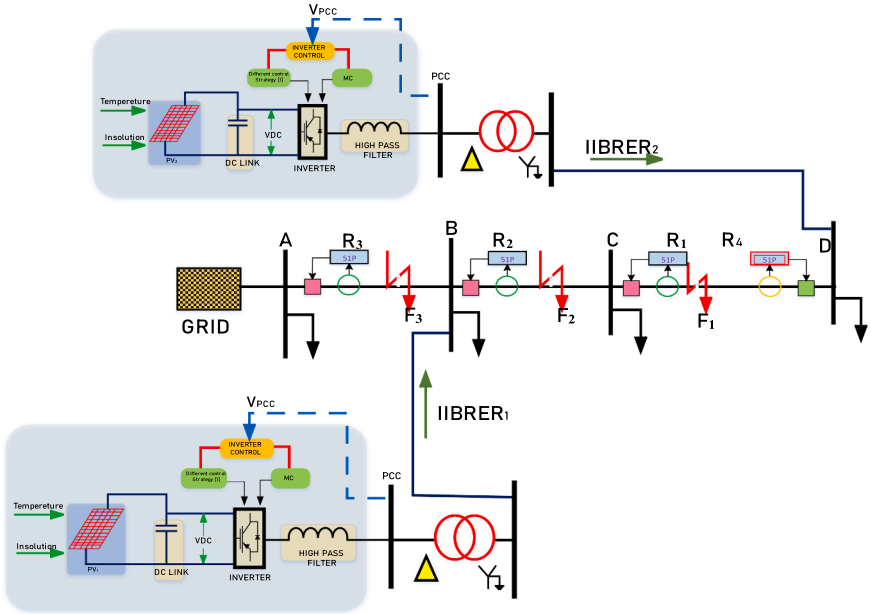

Fig. 5. Single line diagram of the power network equipped with PVs and three fault scenarios.

faulted phase currents being smaller than healthy phase currents. Fig. 6 provides a clearer representation of the positive network during fault case F1 [27,28]. By applying Kirchhoff's current law and considering Eqs. (2)–(5), it becomes evident that the fault current contributed by IBRER directly impacted the fault characteristics, where ΔI^{+}_{R1}, ΔI^{+}_{R2}, ΔI^{+}_{R3} and ΔI^{+}_{R4} are the fault current components at R1to R4, respectively, while R_f is the fault resistance Fig. 6.

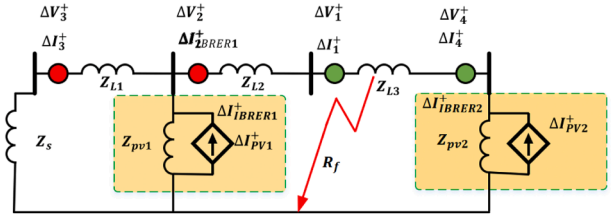

Fig. 6. A positive sequence network of the DN when an internal fault occurs at point F1.

$$I^{+}_{F1} = \Delta I^{+}_{R3} + \Delta I^{+}_{R4} \quad (2)$$

$$\Delta I^{+}_{R4} = \Delta I^{+}_{IBRER2} \quad (3)$$

$$\Delta I^{+}_{R2} = \Delta I^{+}_{R1} + \Delta I^{+}_{IBRER1} \quad (4)$$

$$\Delta I^{+}_{R3} = \Delta I^{+}_{R2} \quad (5)$$

The line impedance is represented by Z_L, and Z_S denotes the equivalent impedance of the power supply. The I^{+}_{F1} represents the fault current at the fault point (F1), while I_{IBRER1} and I_{IBRER2} represent the fault current components contributions of PV1 and PV2 to the fault point. The fault current magnitude ΔI^{+}_{IBRER1} and ΔI^{+}_{IBRER2} are determined by multiple factors, including the intermittent nature of RERs, variations in positive sequence voltage ΔV^{+}_{R2} and ΔV^{+}_{R4}, respectively, by the control function f,

as described in Eqs. (6) and (7).

$$\Delta I^{+}_{IBRER1} = f\left(\Delta V^{+}_{R2}\right) \tag{6}$$

$$\Delta I^{+}_{IBRER2} = f\left(\Delta V^{+}_{R4}\right) \tag{7}$$

The control strategy, mode A, described by Eq. (8) shows a limitation of 2.0 p.u on the controlled fault current, determined by the PCC voltage, V^{+}_{PCC} [23]. Fig. 7a demonstrates the relationship between the current supplied by the IBRER (I_{IBRER}) and V^{+}_{PCC}. Specifically, if the bus voltage falls within the range of 0.9 to 1.1 p. u, the current is reduced to 1.0 p.u. This control characteristic ensures that the fault current remains within specified limits based on the PCC voltage. While the control strategy, referred to as MC, described by Eq. (9) [19,29], dictates that the inverter ceases to supply current when the PCC voltage, (V^{+}_{PCC}) drops below a specific threshold. Fig. 7b illustrates the relationship between the current output from the IBRER and V^{+}_{PCC}, specifically, if the bus voltage falls below 0.5 p.u, the inverter enters the MC mode, ceasing current output entirely. This control characteristic ensures that the inverter protects itself by halting its contribution to the grid when voltage levels indicate a fault or instability in the system. The voltage range for the MC mode, specifically defined as $V < 0.50$ p.u. and $1.10 < V < 1.20$ p.u., is carefully chosen to ensure system reliability, stability, and safety. These thresholds align with both the operational requirements of electrical systems and international standards.

In the low-voltage range ($V < 0.50$ p.u.), this threshold ensures protection against voltage collapse, which typically occurs during severe contingencies such as overloading or network faults. When the voltage drops below this limit, the system is at risk of entering an unstable state due to inadequate power delivery to connected equipment. Operating under such conditions may also damage sensitive components, such as transformers and motors, by causing excessive current draw, which results in overheating and potential insulation failure. Furthermore, equipment designed for operation at nominal voltage levels generally cannot maintain efficiency or functionality at such a low voltage, leading to increased power losses and degraded performance. This range is therefore excluded to maintain the safety and efficiency of the system.

In the high-voltage range ($1.10 < V < 1.20$ p.u.), the upper threshold accounts for potential overvoltage conditions that may arise due to sudden load rejection, poor voltage regulation, or malfunctioning reactive power compensation equipment. Sustained operation within this range poses significant risks, including insulation breakdown of equipment and overexcitation of transformers, which can lead to thermal damage. Additionally, high voltages increase the likelihood of equipment stress and arcing phenomena, potentially leading to system-wide instability. Standards such as IEEE 519 and IEC 60,038 recommend voltage operating limits that allow for slight deviations from nominal levels, typically ±10 %, to accommodate short-term fluctuations without causing damage. The chosen range reflects these recommendations while balancing operational flexibility with equipment protection. By limiting the MC mode to these specified ranges, the system achieves a balance between ensuring the reliable delivery of power and protecting infrastructure from extreme conditions. The thresholds are thus consistent with industry best practices and international guidelines for voltage regulation in power systems.

The MC in the proposed strategy follows the guidelines and requirements outlined in IEEE Std 1547–2018 [30,31]. The IEEE Std 1547–2018 standard specifies the conditions and operational framework under which MC is mandatory, ensuring alignment with established grid codes and regulatory requirements.

$$I_{IBRER} = \begin{cases} 2I_{rated} & 0 \le \left|V^{+}_{PCC}\right| \le 0.9 \\ I_{rated} & 0.9 < \left|V^{+}_{PCC}\right| \le 1.1 \end{cases} \tag{8}$$

$$I_{IBRER(MC)} = \begin{cases} 0 & 0 \le \left|V^{+}_{PCC}\right| \le 0.5 \\ I_{rated} & 0.5 < \left|V^{+}_{PCC}\right| \le 1.1 \\ 0 & 1.1 < \left|V^{+}_{PCC}\right| \end{cases} \tag{9}$$

Fig. 8 demonstrates the impact of MC on the operation of the OCR protection scheme highlights the relay's operating zones and illustrates that the MC mode results in the inverter ceasing to supply any fault current (i.e., inverter output current is effectively zero). This directly implies that the operating zone of the relay is detached from the inverter's contribution when it enters the MC mode. Examining the diagram further, the black dashed line, labelled as Ip represents the rated current of the inverter. Ideally, the OCR is not supposed to respond to this normal inverter current, as it is within safe operational limits. The red line indicates the voltage threshold that triggers the inverter's transition into MC mode. This voltage drop reflects the critical point at which the inverter ceases to supply current, leaving it effectively disconnected from fault contributions.

When analyzing the interaction between the relay's characteristic curve and the voltage drop during the fault, it becomes evident that if the OCR is responsible for protecting the inverter from faults occurring downstream, it will not detect any fault current from the inverter during

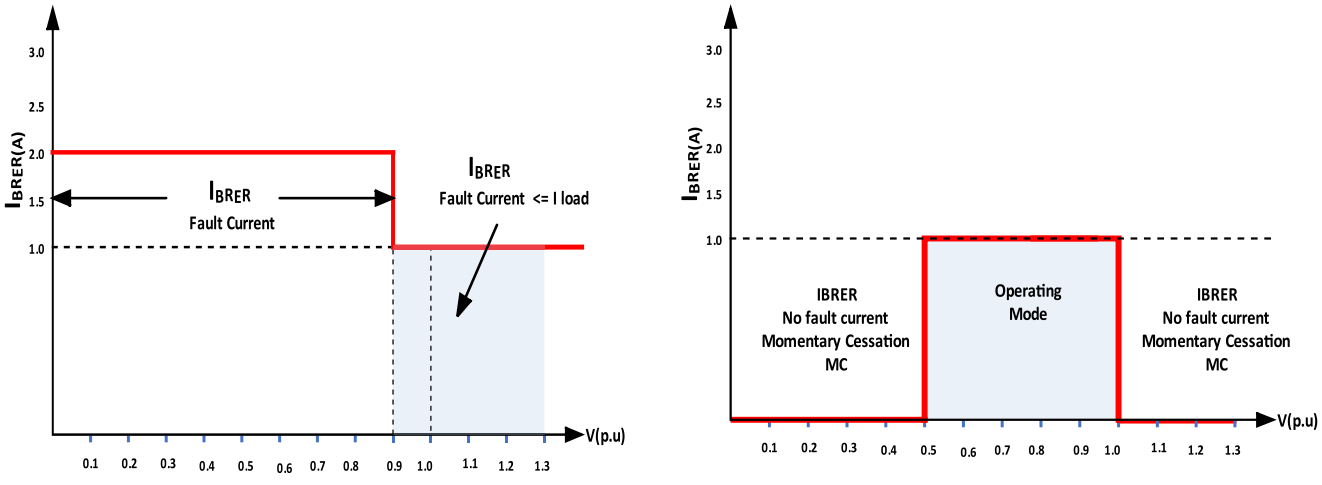

a. Normal control operation

b. MC operating mode

Fig. 7. Control mode with and without MC.

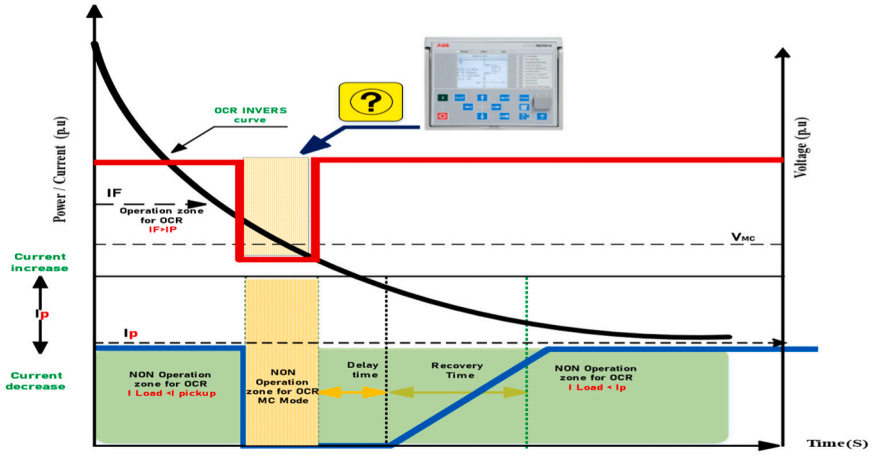

Fig. 8. Overcurrent operation regions with MC enabled under varying busbar voltage conditions connected to the PV inverter.

the MC mode. This is because the inverter's contribution drops to zero, and thus the relay cannot issue a tripping command since the fault current never exceeds the relay's pickup setting, Ip .

In such cases, the inverter relies entirely on its internal protection mechanism via MC, preventing any contribution to fault clearance through the relay. Conversely, if the OCR is situated farther upstream or on a different bus from where the inverter is connected, the relay will still detect the fault current sourced from the utility grid. In this scenario, the relay can respond to the fault, issuing a trip command and isolating the faulted section regardless of the inverter's behavior. This means the relay continues to operate effectively by clearing the fault using grid-supplied current, even when the inverter enters the MC mode.

2.4. The proposed advanced OCR protection approach

The integration of IBRERs into modern power systems presents unique challenges for protection schemes. One critical issue is the transition of inverters into MC mode during fault conditions, as discussed in Sections 2.1 and 2.2. The transition into MC significantly affects the relay's ability to detect and respond to faults involving the inverter. Therefore, ensuring proper coordination between the inverter's protection mechanisms and the OCR settings is crucial for maintaining reliable fault protection in systems with inverter-based resources. To address this issue, a proposed advanced OCR protection solution based on voltage and current measurements is introduced in Eq. (10). The proposed equation establishes a unified approach for adaptive protection in electrical systems. It integrates two components, the standard inverse OCR component and the voltage-controlled MC component to ensure precise and efficient response times during fault conditions. The equation incorporates a unit step function, as described in Eq. (11) to facilitate seamless switching between these components, optimizing system performance and enhancing robustness.

$$t_r = \left[\left(\frac{0.14*TMS}{\left(\frac{I_f}{I_p}\right)^{0.02}-1}\right).\delta\right] + \left[\left(\frac{0.14*TMS}{1-\left(\frac{V_f}{V_0}\right)^{0.02}}\right).(1-\delta)\right] \quad (10)$$

$$\delta = U(V_f - 0.5) - U(V_f - 1.1) \quad (11)$$

The tripping time (t_r) of the OCR is determined by dynamically activating either the standard inverse OCR component, $\left(\frac{0.14*TMS}{\left(\frac{I_f}{I_p}\right)^{0.02}-1}\right)$ as described in Eq. (1) or the voltage-controlled MC component, $\left(\frac{0.14*TMS}{1-\left(\frac{V_f}{V_0}\right)^{0.02}}\right)$, depending on the fault voltage (V_f). The Unit Step Function (U) directs this switching logic, ensuring that the appropriate protection mechanism is engaged under varying fault conditions. Firstly, the standard inverse OCR component, which becomes active when the fault voltage lies within the range $0.5 < V_{Fault} < 1.1$. The response time for this component is calculated as a function of the fault current (I_{Fault}) relative to the pickup current (I_p). The TMS adjusts the overall response delay and the response time is inversely proportional to the ratio $\frac{I_f}{I_p}$. This formulation ensures that higher fault currents result in shorter response times, promoting prompt action during severe fault conditions. Secondly, the voltage-controlled MC component becomes active when the fault voltage is either less than or equal to 0.5 or greater than or equal to 1.1. The response time for this component is determined as a function of the normalized fault voltage (V_f), where V_0 is a reference voltage. This component addresses scenarios where the voltage deviates significantly from nominal values, allowing the protection system to adapt to MC conditions. Fig. 9 displays the tripping time characteristics of the inverse OCR as a function of the fault current (I_f). The curve follows the standard inverse time-current relationship (first component), with TM fixed at 0.5. On the x-axis, the fault current is represented in p.u, while the y-axis denotes the relay's operating time in seconds. Red markers are used to highlight specific fault current values (I_f= 1.5, 2.5 and 3.5 p.u), each corresponding to its respective operating time on the curve. Fig. 8 illustrates how the relay's operating time decreases non-linearly as the fault current increases, reflecting the essential characteristic of inverse OCR, which ensures faster tripping at higher fault currents. This feature is critical for system protection against excessive currents. On the other hand, Fig. 10 illustrates the operating time characteristics of the second

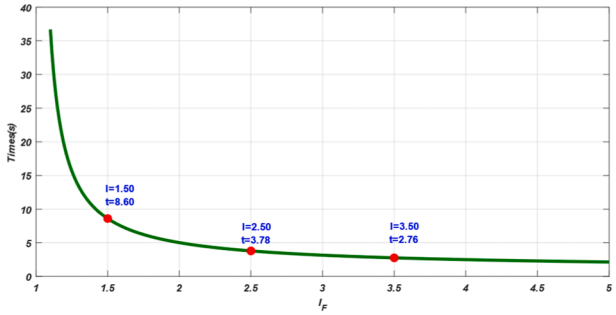

Fig. 9. Operating time of the inverse OCR as a function of fault current (TMS = 0.5).

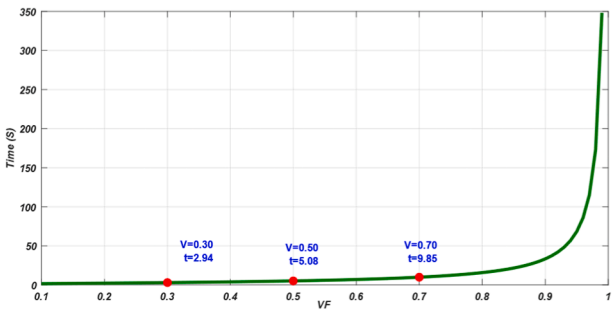

Fig. 10. Operating time of the voltage protection relay as a function of fault voltage (TMS = 0.5).

component based on the voltage, as a function of the fault voltage (V_f) with TMS is set at 0.5. The x-axis represents the fault voltage in p.u, while the y-axis shows the relay's operating time in seconds. Red markers highlight specific fault voltage points (V_f = 0.3, 0.5 and 0.7 p.u), with each point corresponding to its associated operating time. The curve follows the voltage-controlled inverse time relationship, where the relay's operating time increases as the fault voltage approaches the reference voltage (V_0). This behavior highlights the adaptive nature of voltage protection relays in response to deviations from nominal voltage conditions.

3. System description and results

3.1. System description

This study utilizes the CIGRE 14-bus DN, whose comprehensive specifications are shown in Fig. 11 and are accessible in [32]. The network operates with a high-voltage/medium-voltage (HV/MV) utility source and includes two 10 MW photovoltaic (PV) farms, each connected via a step-up transformer rated at 0.4/12.49 kV. Each 10 MW farm is composed of ten 1 MW PV systems and controlled by control configuration as described in Tables 1 and 2. The characteristics of the OCRs, current transformer (CT) ratio and pickup current, of the CIGRE network are provided in Table 3.

3.2. Simulation results

OC Protection is widely used in both transmission and distribution networks, serving as one of the primary lines of defence for protecting transformers, cables, and other electrical equipment. The design and coordination of protection devices are integrated to operate cohesively with other protective mechanisms, ensuring a fast and accurate response to various fault conditions. Achieving proper coordination is crucial for establishing an effective and reliable protection system within the electrical network. The following case studies use the CIGRE 14-bus DN, which incorporates RERs, to evaluate the impact of MC on the operation

Table 1
Inverter parameters.

Parameter	Value
DC Rating (MW)	1.5
DC Voltage (V)	1880
Vmax (%)	110
Vmin (%)	0
FLA (Full Load Amps)	797.9
Efficiency at 100 % Load (%)	90
Efficiency at 75 % Load (%)	90
Efficiency at 50 % Load (%)	90
Efficiency at 25 % Load (%)	90
Imax (%)	105
AC Rating (MVA)	1.35
AC Voltage (kV)	2
FLA (Full Load Amps)	389.7
Normal Operating Voltage - Vmin (%)	90
Normal Operating Voltage - Vmax (%)	110
Minimum Power Factor (PF)	80
Maximum Power Factor (PF)	100

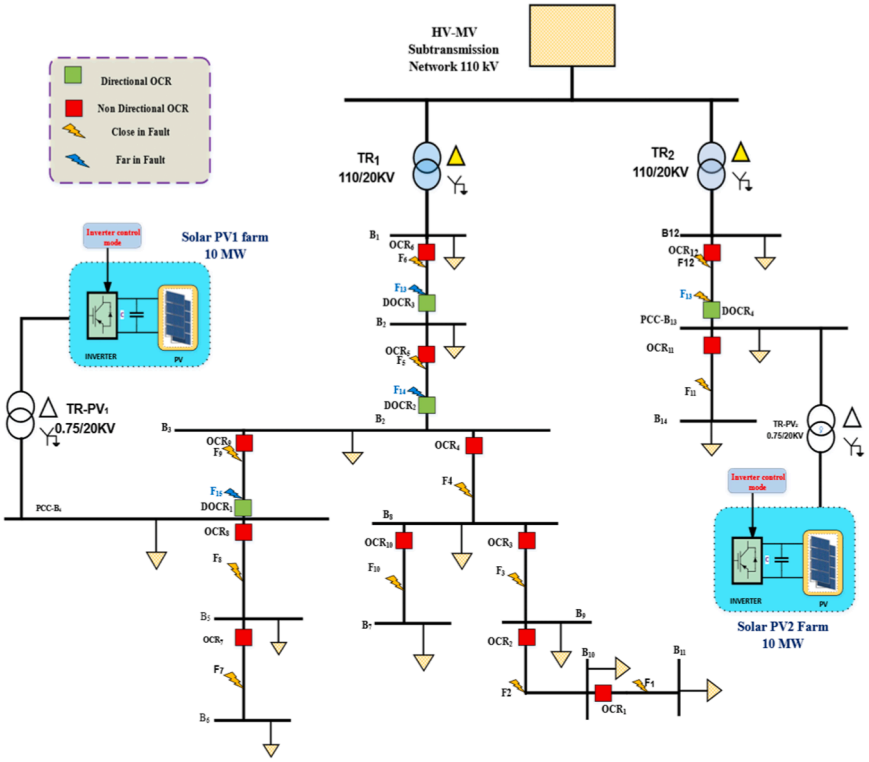

Fig. 11. CIGRE 14-bus distribution network.

Table 2
Inverter control mode parameters: with and without MC.

Parameter	MC control mode	Normal Control Mode
Voltage	0 % - 90 V - 110V	0 % - 50 V - 110V
S.C. Current	200 % - 110 % - 100 %	200 % - 110 % - 100 %
Vs-max	0 %	50 %
Vop-min	90V	90V
Vop-max	110V	110V
Isc-max	200 %	200 %
Reactive Current Priority	Enabled	Enabled
Real Power Priority	Disabled	Disabled

Table 3
CT Ratio and current settings.

OCR	CT ratio	pickup current (A)
OCR 1 to 4	200/1	50
OCR 5 and 6	200/1	150
OCR 7 to 12	200/1	50
OCR 13 to 16	300/1	300

of the OC protection system:

- Case #1: The model simulation results without IBRERs.
- Case #2: The model simulation results using IBRERs without MC.
- Case #3: The model simulation using IBRERs with MC
- Case#4: The model simulation in the event of an islanding mode with MC.

3.2.1. Simulation results of Case #1

The protection scheme of the CIGRE network includes 12 OCRs, with primary and backup relays assigned to twelve fault locations, labelled from F1 to F12. These fault locations cover both near- and far-end points from the sources, allowing the assessment of different PV operating control scenarios and their impact on fault detection and protection schemes. To ensure precise operation, initial load flow and fault analysis are conducted to determine the CT ratios and relay pickup currents following the IEC-60,909 standard. In this study, the TMS for each OCR is optimized based on the maximum line load currents and various fault scenarios, including three-phase short circuits (LLL faults). To guarantee prompt activation of the primary OCRs, the CTI is set to 0.3 S [10]. Additionally, the OCR pickup current is configured to 1.2 times the full load current. These parameter settings are essential for ensuring fast and reliable OCR operation, taking into account load characteristics and fault scenarios. Table depicts the results of Case#1. From a protection engineer's perspective, the overall coordination scheme appears to be well-designed and effectively implemented across the network. The primary objective of relay coordination is to ensure selective isolation of faults while minimizing disruption to the rest of the system. The fact that most relay pairs achieved the 0.3 S, CTI demonstrates that the system provides adequate selectivity and reliability.

In most fault scenarios, the CTI between the main and backup relays is within the acceptable 0.3 S period, showing that the relay settings are properly configured to provide selectivity and fault clearance, as shown in Table 4. In addition, faults F9 and F10 show that the CTI between primary and backup relays does not reach the required 0.3 S. However, this does not imply a failure to coordinate. The coordination process ensures that the backup relay operates if the primary relay fails. For both F9 and F10, R5 serves as the backup for both R9 and R4. Coordination is primarily achieved between R5 and R4 since they share the same bus. As a result, the coordination between R5 and R9 is implicitly ensured once the slower relay, R4, is properly coordinated. Similarly, R4 acts as backup protection for both R3 and R10. Coordination is first established between R4 and R3, which ensures that the coordination between R4 and R10 is automatically achieved. This setup guarantees effective fault isolation, ensuring that the backup relay intervenes only when the primary relay fails, thus maintaining the overall reliability and selectivity of the protection system. This indicates that the network's protection system still preserves selectivity and reliability since the coordination is formed indirectly through common relay pathways. These examples highlight how difficult it may be to maintain coordination when relays are linked together and that there are still network topologies are obtaining the CTI indirectly is possible. For faults F6 and F12, relays R6 and R12 are the last relays in the network, with the transformer relay being the only remaining protective device. As such, these relays have no backup relays available, which explains the absence of a recorded CTI. This is a typical scenario in radial networks where the end relays act as the final line of defence. It's a reminder of the importance of ensuring that these final relays are robust and capable of handling faults without the need for further backup.

The fault current magnitude and CTI values over 12 fault locations (F1 to F12) are shown in Fig. 12(a).

From the figure, it is depicted that most fault sites have very steady fault current values, except for F5, F9, and F12, which have large spikes. F5 has a peak fault current of roughly 2901 A, indicating a significant short-circuit contribution, whereas F9 has a fault current of approximately 1541 A. F12 has the largest fault current, exceeding 6624 A, making it the most severe fault in terms of current magnitude. These variations in fault current can be attributed to the proximity of the fault to the power source and the network impedance at different locations. However, it is important to note that the faults with the highest fault currents (F5, F6, and F12) do not have backup protection because they occur at the last protective relay in the system as cleared in Fig. 12(b). This absence of backup protection at these locations makes the system more vulnerable and may lead to extended fault-clearing times. For most locations, the CTI values remain consistent, hovering around 0.3 S. However, F9 shows a significant deviation, with the CTI increasing to

Table 4
Relay operation Case Conventional mode under Case #1.

Fault Location	Fault Current (A)		Relay Pairs		TMS		Operating time (s)		CTI
	Primary (A)	Backup (A)	Primary Relay	Backup Relay	Primary TMS	Backup TMS	Primary (s)	Backup (s)	
F1	1230.0	1230.0	R1	R2	0.025	0.168	0.053	0.356	0.303
F2	1316.0	1316.0	R2	R3	0.168	0.313	0.348	0.647	0.299
F3	1355.0	1355.0	R3	R4	0.313	0.458	0.641	0.941	0.299
F4	1541.0	1541.0	R4	R5	0.458	0.492	1.141	1.443	0.302
F5	2901.0	2901.0	R5	R6	0.492	0.622	1.128	1.427	0.299
F6	6618.0	6618.0	R6	No backup	0.622	…	1.107	…	1.107
F7	1371.0	1371.0	R7	R8	0.025	0.180	0.051	0.368	0.317
F8	1448.0	1448.0	R8	R9	0.171	0.320	0.344	0.643	0.299
F9	1541.0	1541.0	R9	R5	0.320	0.492	0.631	1.443	0.812
F10	1335.0	1335.0	R10	R4	0.025	0.313	0.052	0.641	0.590
F11	1541.0	1541.0	R11	R12	0.025	0.205	0.050	0.348	0.299
F12	6624.0	6624.0	R12	No backup	0.205	—	0.280	…	0.280

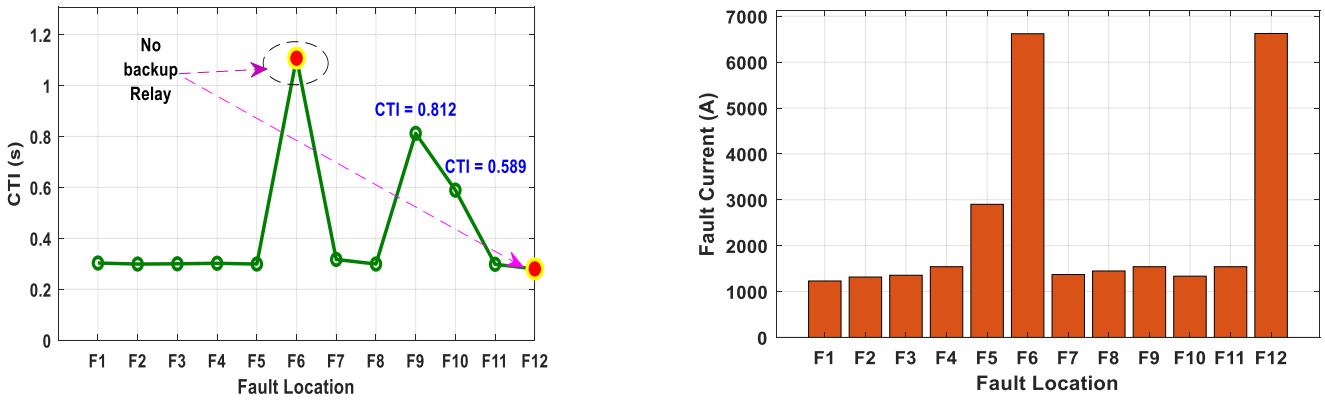

a. CTI values for all fault locations

b. Fault current against fault locations

Fig. 12. Fault current magnitude and CTI value over 12 fault locations (Case#1).

0.6 S, followed by a sharp drop to 0.2 S at F10. This indicates a delay in fault clearing time at F9, potentially due to the absence of backup protection. The longer CTI suggests that the system's protection coordination is stressed when faults occur in the final relays, such as F9 and F12. The lack of backup protection at these high-fault current locations, combined with the sharp CTI fluctuations at F6 and F12, highlights the critical importance of ensuring optimized protection settings for these fault areas.

Furthermore, Fig. 13 illustrates the coordination achieved during F3, specifically between R3 and R4, where a CTI of 0.3 S is realized. In contrast, the coordination between R4 and R10 during F10 resulted in a CTI of 0.594 s, attributed to the coordination between R4 and the slower relay. Fig. 14 depicts the relation between the operating time (S) for each relay pair, which is critical in clearing faults at specific locations in the network, under different fault conditions. From Fig. 14, it is remarked that there are significant variations in operating times across the different relay pairs. Relay pairs F4, F5, F6, and F9 exhibit the longest operating times, reaching up to 1 S in some cases. These relays take longer to respond, which could suggest that faults in these locations either have higher severity or that the relay settings are designed to allow more time for primary protection to act before the backup relays are triggered. Conversely, relay pairs F1, F11, and F12 have the shortest operating times, around 0.1 to 0.2 S, indicating that they respond quickly to faults in these locations. The quicker response times in these locations might suggest that these faults are closer to the source, or that the system design prioritizes faster fault clearance in these areas to maintain grid stability.

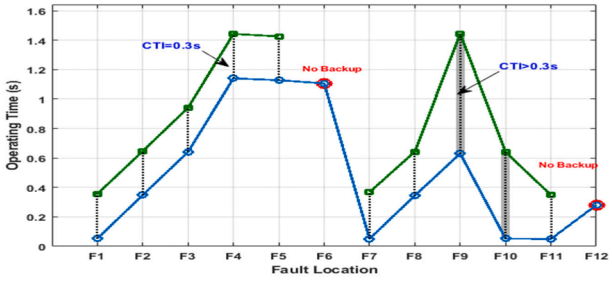

Fig. 14. Relationship between operating time and relay pairs.

3.2.2. *Simulation results of Case# 2*

Table 5 and Fig. 15 investigate the impact of integrating 10 MW solar PV units at busbars 4 and 13 on the overall performance of the electrical protection system. The results indicate that the introduction of these PV units has a significant influence on the protection system's operation, particularly on the OC protection relays and coordination between primary and backup protection devices. Firstly, the addition of the PV sources has led to an increase in the fault current values, as evident in several fault locations. For instance, at fault location F4, the primary fault current is observed to be 2295 A, with the backup current reaching 1568 A, indicating a substantial contribution from the PV units. This

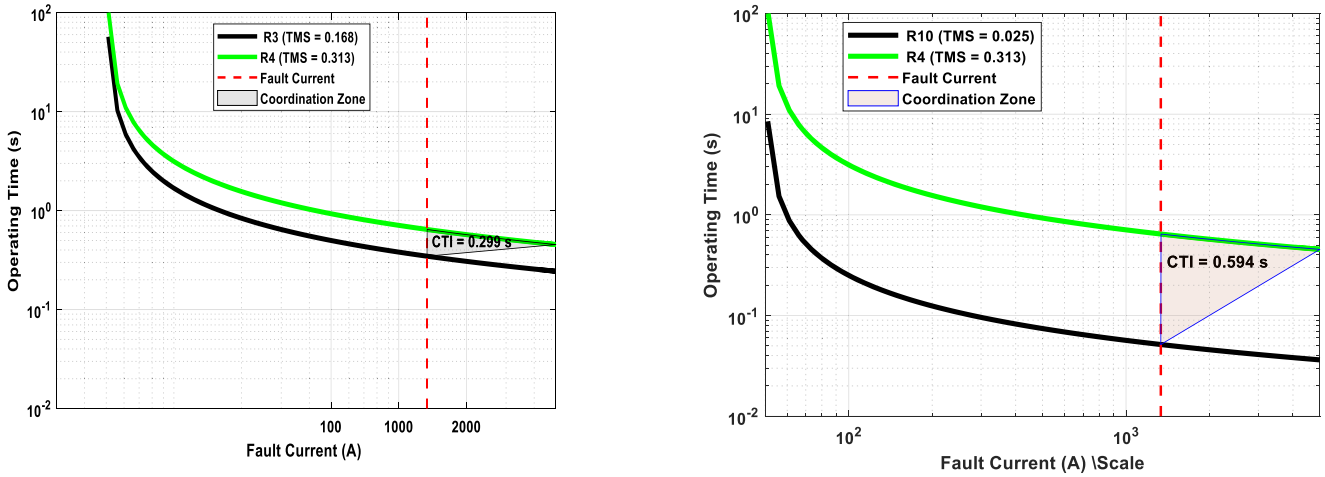

a. Coordination between R3 and R4 for F3

b. Coordination between R10 and R4 for F10

Fig. 13. Fault case F3 andF10.

Table 5
PV farms' effects on OC protection without taking MC.

Fault Location	Fault Current (A)		Relay Pairs		TMS		Operating time (s)		CTI
	Primary (A)	backup (A)	Primary Relay	backup Relay	Primary TMS	backup TMS	Primary (s)	backup (s)	
F1	1559	1559	R1	R2	0.025	0.168	0.053	0.330454052	0.2775
F2	1956	1956	R2	R3	0.168	0.313	0.309298	0.574988584	0.2657
F3	2014	2014	R3	R4	0.313	0.458	0.570274	0.836340649	0.2661
F4	2295	1568	R4	R5	0.458	0.492	0.992121	1.432410114	0.4403
F5	2949	2949	R5	R6	0.492	0.622	1.121471	1.41888772	0.2974
F6	6711	6711	R6	No backup	0.622	…	1.107	…	1.107
F7	2082	2082	R7	R8	0.025	0.18	0.0452	0.309532694	0.2643
F8	2198	1470	R8	R9	0.171	0.32	0.304929	0.640379352	0.3355
F9	1568	0.779	R9	R5	0.32	0.492	0.32	1.443	1.123
F10	2014	2014	R10	R4	0.025	0.313	0.0251	0.641	0.6159
F11	3422	2663	R11	R12	0.025	0.205	0.039685	0.346998747	0.3073
F12	6709	0.82	R12	No backup	0.205	—-	0.28	…	0.28
F13	648	648	DOCR3	DOCR2	0.025	0.086	0.123	0.424	0.301
F14	734	734	DOCR2	DOCR1	0.086	0.088	0.393	0.693	0.3
F15	735	—-	DOCR1	No backup	0.088	—-	0.682	…	0.682
F16	764	—-	DOCR4	No backup	0.025	—-	0.742	…….	0.742

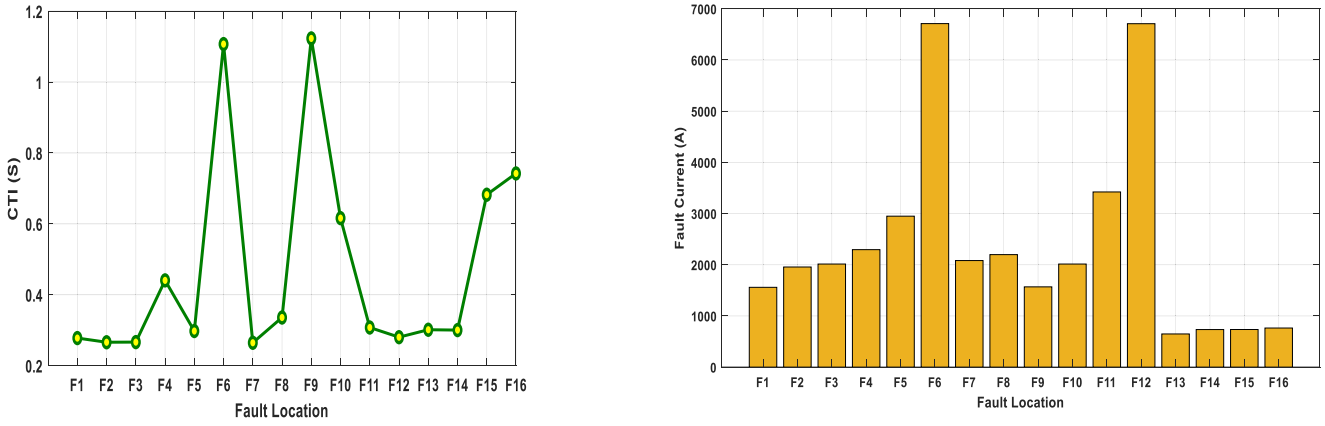

a. CTI values for all fault locations

b. fault current against fault location

Fig. 15. Fault current magnitude and CTI value over 12 fault locations (Case#2).

influence is even more pronounced in fault F6, where the fault current surges to 6711 A without any backup relay being available, showing the potential impact on relay operations due to the increased contribution of IBRERs. To address this impact, directional Overcurrent Relays (DOCR1 to DOCR4) are introduced, which are crucial in handling the reverse fault current contributions induced by the PV units. These relays help maintain the CTI within the permissible limit of 0.3 S at fault locations F13, F14, F15, and F16. However, the results clearly show that the introduction of IBRERs has disrupted the coordination between relays, which is a critical aspect of maintaining reliable protection in the system.

For example, at fault F13, the primary relay DOCR3 operates in 0.123 S, while the backup relay DOCR2 takes 0.424 S to clear the fault, resulting in a CTI of 0.301 S, which is just within the acceptable range. Nevertheless, the data shows that at fault locations F15 and F16, there are no backup protection relays available, as these represent the terminal points of the network. This absence of backup protection emphasizes a vulnerability in the system, suggesting that the PV integration requires further adjustment of the protection scheme. Furthermore, analyzing the TMS and operating time values reveals that the TMS settings need careful calibration when integrating IBRERs. For instance, at fault F5, the primary relay R5 has a TMS of 0.492, resulting in an operating time of 1.121 S, while the backup relay R6 has a TMS of 0.622 with an operating time of 1.418 S. The difference in CTI here is around 0.297 S, which is quite close to the coordination threshold. The results demonstrate that with the inclusion of PV generation, especially as seen at F4 and F13, the system's ability to maintain the necessary CTI is challenged, and maintaining proper coordination becomes increasingly difficult due to the altered fault current flows. This observation reinforces the need for careful recalibration of relay settings and consideration of reverse power flows introduced by the PV systems.

3.2.3. *Simulation results of Case #3*

Table 6 presents the results of the simulation conducted to analyze the influence of MC on the OC protection system in the utility grid. The table records the PV PCC voltages, which assist in determining if the inverter has entered the MC mode during faults. The impact of the MC mode on the protection system is observed, especially during reverse faults at F13, F14, F15, and F16. In these fault conditions, the currents from the inverters drop to zero due to the inverter entering the MC mode, which means that the OC protection does not activate as the fault current is effectively zero. Therefore, deciding whether to disconnect the inverter through the Overcurrent Relay becomes a challenge during this period.

Fig. 16 illustrates fault case F1 and its impact on the coordination between R1 and R2. As shown in Fig. 16(a), the activation of the inverter in MC mode at the moment of the fault does not affect the coordination between the relays and keeps a constant CTI of about 0.303 S. However,

Table 6
The impact of MC on OC protection.

Fault	Fault Current (A)		Relay Pairs		PCC Voltage		Operating time (s)		CTI
Location	Primary (A)	backup (A)	Primary Relay	backup Relay	PV1 Bus 4 %	PV2 Bus 13	Primary (s)	backup (s)	
F1	1251	1251	R1	R2	22	107	0.053	0.353830891	0.3008
F2	1251	1251	R2	R3	16	107	0.346358	0.643883689	0.2975
F3	1378	1378	R3	R4	13	107	0.637974	0.935627802	0.2977
F4	1568	1568	R4	R5	0	107	1.133784	1.432410114	0.2986
F5	2949	2949	R5	R6	0.14	107	1.121471	1.41888772	0.2974
F6	6711	No backup	R6	No backup	0.232	94	1.107	…	1.107
F7	1395	1395	R7	R8	5.6	108	0.050844	0.348177315	0.2973
F8	1474	1474	R8	R9	0.18	108	0.342318	0.639847492	0.2975
F9	1568	0.779	R9	R5	13.75	108	0.32	1.443	1.123
F10	1378	1378	R10	R4	104	108	0.0251	0.641	0.6159
F11	2666	2663	R11	R12	98	0	0.042284	0.346998747	0.3047
F12	6709	No backup	R12	No backup	98	0	0.28	…	0.28
F13	0	0	DOCR3	DOCR2	0.18	110	No Trip	No Trip	
F14	0	0	DOCR2	DOCR1	0	107	No Trip	No Trip	
F15	0	—-	DOCR1	No backup	0	107	No Trip	No backup	
F16	0	—-	DOCR4	No backup	104	0	No Trip	No backup	

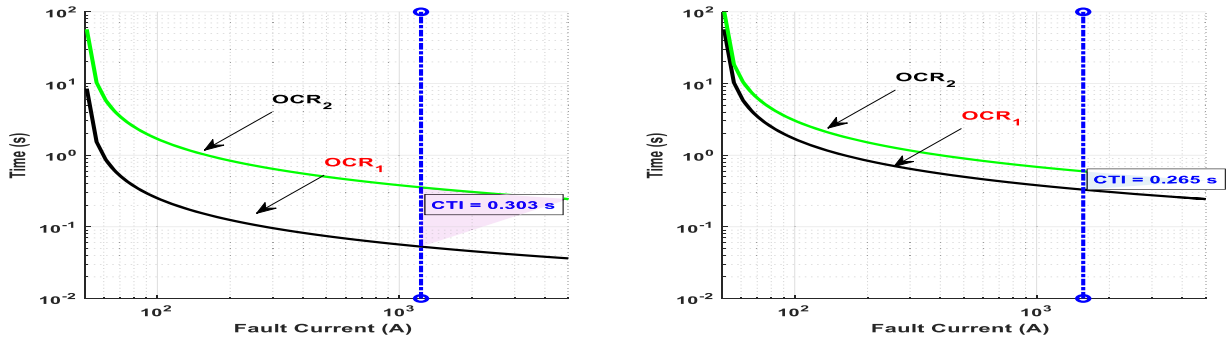

a. Relay pairs R1andR2 CTI values under Case# 3 without IBRER

b. Relay pairs R1andR2 CTI values under Case# 3 with IBRER

Fig. 16. F1′s effect on R1 and R2′s coordination in Cases 3.

when the inverter contributed to the fault current, miscoordination occurred with 0.265 S, as depicted in Fig. 16(b).

Figs. 17 and 18 illustrate the variations in fault current waveforms and RMS responses under two operating scenarios. In the first scenario, depicted in Fig. 17, the system operates in MC mode. During this mode, a fault occurs at $t = 2.0$ S, triggering relay R1 to activate at $t = 2.053$ S, followed by R2 at $t = 2.353$ S. This sequence establishes a CTI of 0.3 S between the two relays, ensuring a smooth and orderly protection transition. Fig. 18 represents the system's performance without MC control but with IBRER in operation. In this case, the coordination between relays R1 and R2 depends on their independent operating times rather than a predetermined CTI. Upon fault detection at $t = 2.0$ S, relay R1 responds at $t = 2.053$ S, while relay R2 activates at $t = 2.3$ S. This arrangement showcases a dynamic CTI influenced by the relays' response times, highlighting the impact of IBRER integration on the protection system's coordination behavior.

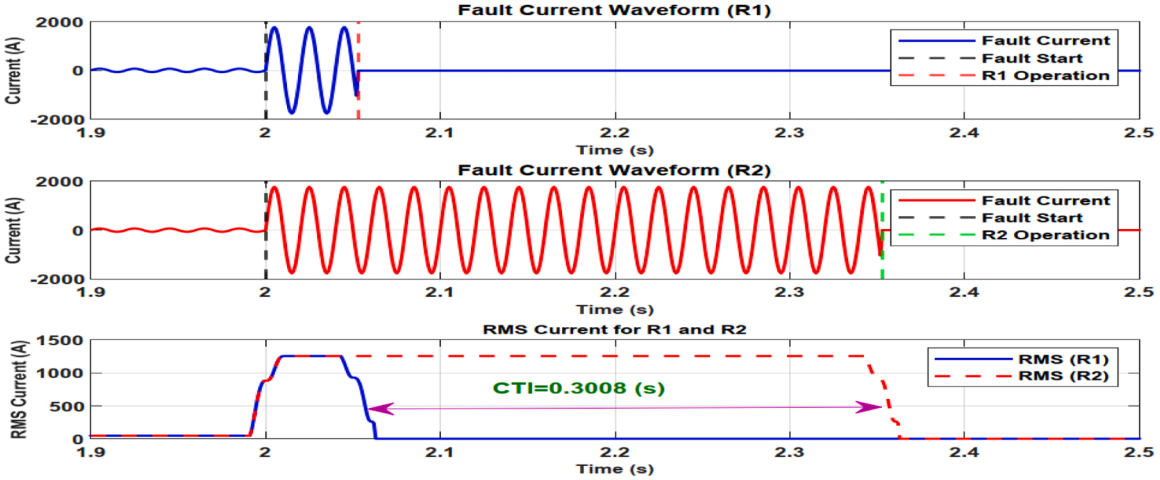

Fig. 17. Relay pairs R1and R2 CTI values under MC mode for F1.

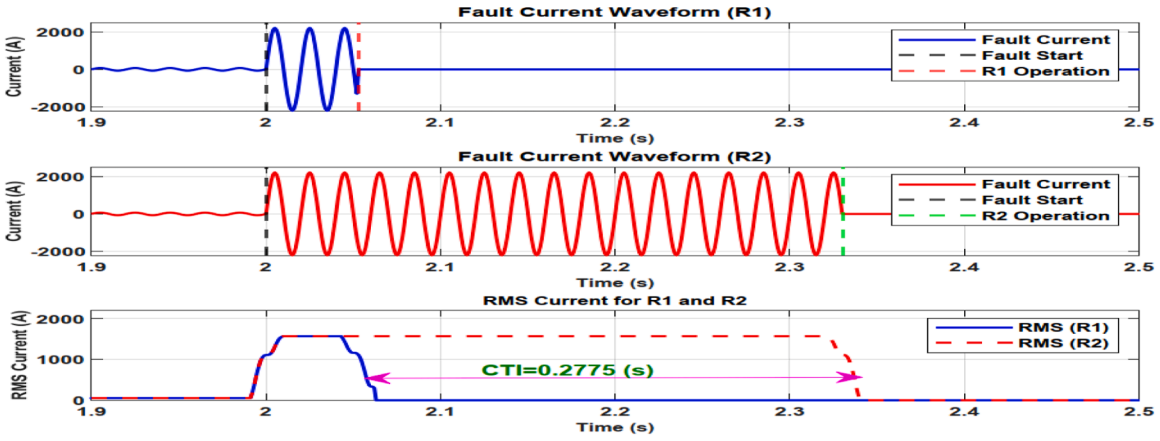

Fig. 18. Relay pairs R1and R2 CTI values without MC mode for F1.

Moreover, the data shows that PV2 enters the MC mode during faults F16, F12, and F11. From a protection standpoint, this mode has contributed to maintaining relay coordination within permissible limits, as evidenced by the CTI values in the table. This is because the inverter's absence from contributing to the fault current helps to preserve the protective coordination, avoiding unnecessary tripping. The results also highlight the yellow-colored faults, F6 and F12, which indicate faults without backup protection since they represent the last relays in the entire system. This reveals a critical vulnerability in the network, emphasizing the need to ensure these terminal relays operate reliably. A crucial observation from the results is that while the MC mode effectively reduces the inverter's contribution to fault current, it also impacts downstream faults like F1, F2, and F3. For example, during a fault at F1, the inverter at Bus 4 enters MC mode, and due to the inverter's settings, it remains in this mode for approximately one second as cleared in Fig. 19(a). This means that even if the primary relay isolates the fault within 0.052 S, the inverter will still wait for the full second before reconnecting to the grid. During this interval, all loads previously fed by PV1 are temporarily supplied by the grid, resulting in an increased current flow through relay R9 to cover the additional load demand, potentially causing it to trip due to overload before the inverter can resume operation. As noted for the reverse faults, no relay operation occurs because the current is effectively zero, leading to an absence of CTI values. These cells are intentionally shaded, reflecting that no coordination interval can be calculated when the fault current contribution is zero as illustrated in Fig. 19(b) for faults F16, F14, F18 and F13.

Fig. 20 illustrates that the introduction of MC enhances relay coordination, as the absence of inverter contribution to the fault current ensures that coordination remains stable, which is a key advantage of MC. This effect is particularly evident at F1 between R1andR2. Conversely, without the implementation of MC in Case# 2, the coordination fails to maintain the required selectivity, as demonstrated in Fig. 20. Additionally, Fig. 21 shows the voltages at buses 13 and 14, highlighting the regions where the inverter enters the MC mode. The fault resistance (RF) plays a significant role in influencing the behavior of inverters during faults, especially regarding their transition into the MC mode. Higher RF tends to limit the fault current, reducing the magnitude of the fault as perceived by the inverter. As a result, the inverter might remain in service longer and avoid entering the MC mode, or it may experience a delayed response before transitioning into MC. This is because the reduced fault current due to higher resistance may not be detected immediately as a severe fault by the inverter's protection settings. Conversely, when the RF is low, the fault current increases, making it more likely for the inverter to detect a significant disturbance in the grid. In such cases, the inverter is more prone to quickly enter the MC mode as a protective measure, resulting in a momentary disconnection from the grid. This quick transition helps protect both the inverter and the overall system from the effects of the

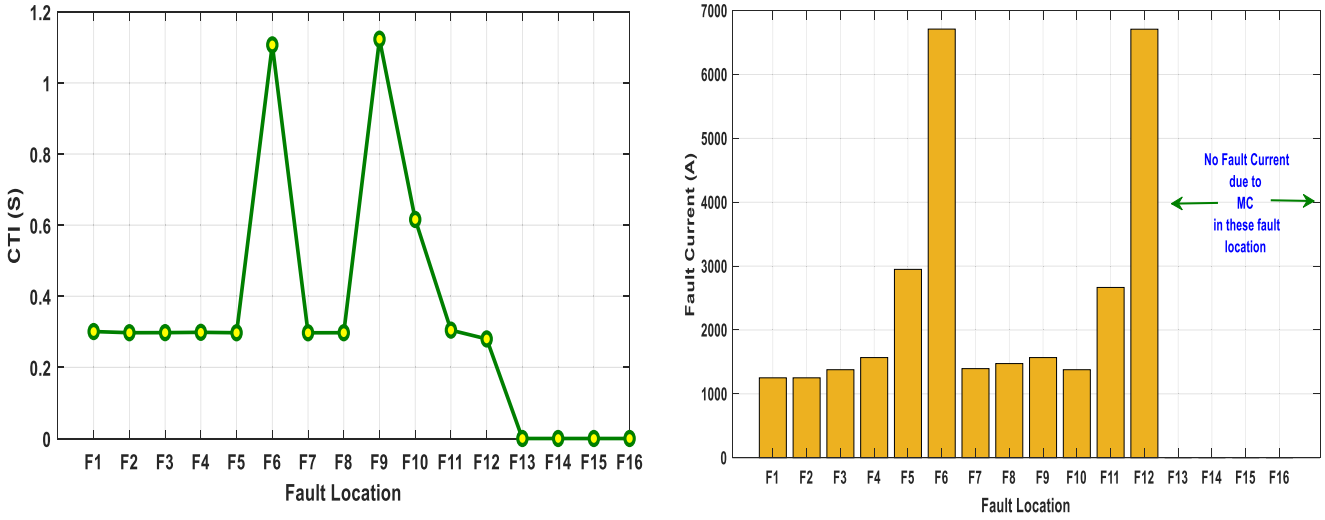

a. CTI values for all fault locations

b. Fault current against fault location

Fig. 19. Fault current magnitude and CTI value over 12 fault locations (Case#3).

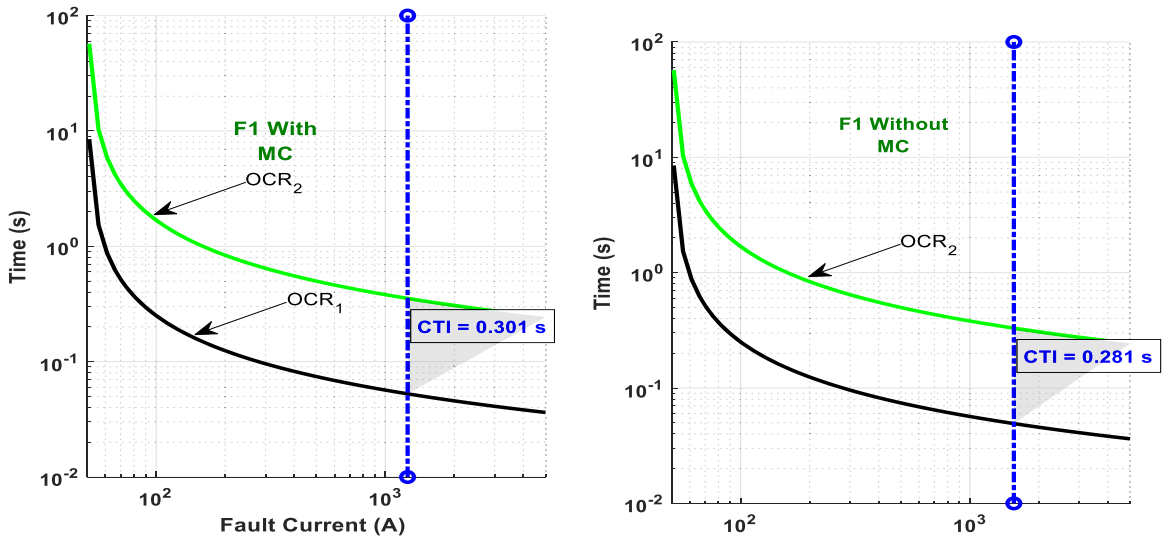

Fig. 20. Fault Case F1 with and without MC operating mode.

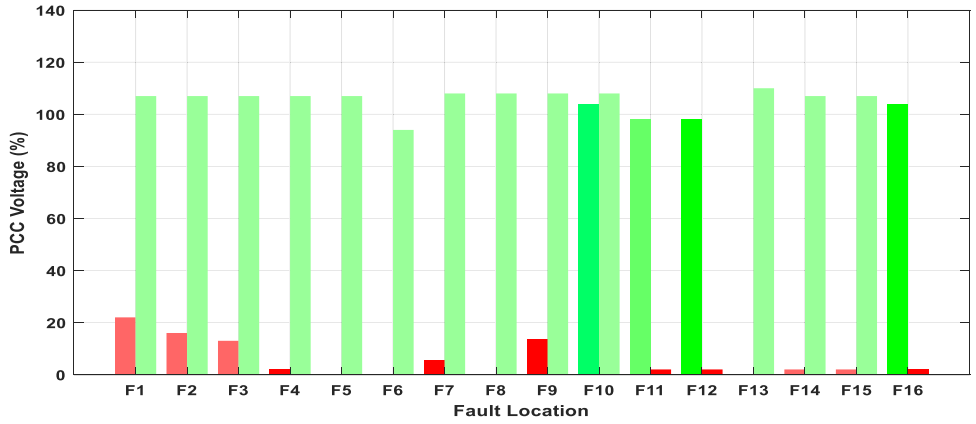

Fig. 21. PCC Voltage at Fault Locations for PV1 and PV2.

high fault current.

Therefore, the level of RF directly impacts the duration and likelihood of the inverter entering MC, affecting overall system stability and the coordination of protection devices during fault conditions. Properly accounting for RF is crucial in ensuring that the protection settings of the inverter respond accurately, maintaining the reliability and safety of the electrical network. Fig. 22 and Table 7 show that RF has a significant impact on the MC behavior of the inverters. As RF increases, the voltage levels at the PCC for both PV1 and PV2 generally rise, reducing the likelihood of the inverter entering the MC mode. For example, at fault location F1, when the RF is 0 ohms, the voltage at PV1 is only 22 %, which is well below the threshold that would trigger MC. However, as RF increases to 20 ohms, the voltage at PV1 rises to 91 %, indicating that the inverter is more likely to stay operational and avoid entering MC.

This pattern is consistently observed across multiple fault locations. At fault F3, for instance, the voltage at PV1 starts at 13 % with RF = 0 ohms and reaches 103 % with RF = 20 ohms, showing that higher resistance helps in maintaining adequate voltage levels at the PCC. Such voltage increases reduce the chances of the inverter entering MC, thereby ensuring a more stable and uninterrupted supply of power. However, fault locations F11 and F12, PV2 shows a voltage of 0 % across all resistance values, indicating that it is not significantly contributing to voltage support in these scenarios. One of the advantages of higher RF is that it prevents the inverter from entering MC by maintaining the voltage above the critical threshold. This means that even during faults, the inverter remains connected to the grid, contributing to overall system stability and reducing power supply interruptions. This behavior is crucial for ensuring that PV systems remain reliable during disturbances.

However, there are also disadvantages associated with increased RF. As RF increases, the fault current decreases, potentially leading to delayed detection and response by the protection system. This delay can impact the overall safety of the electrical network, as the system might take longer to isolate and clear faults. Additionally, reduced fault current contribution from the inverter may affect the coordination between protection devices, especially in networks with multiple sources. It is also evident from Table 7 that PV2 tends to maintain a more stable voltage regardless of the RF in most cases, with values remaining close to or above 100 % for many fault locations, such as F1 and F2.

3.2.4. *Simulation results of Case#4*

In Table 8, the system's behavior under the island mode is analyzed by simulating the disconnection of the main breaker and isolating the loads connected to Bus 1 and Bus 2, which represent other feeders from the grid. It is evident that, in the island mode, the inverters consistently enter the MC mode across all fault locations as cleared in Fig. 23. This behavior indicates that any fault results in the immediate disconnection of PV1 and PV2, effectively rendering the overcurrent protection system inoperative. Since OC protection relies fundamentally on the presence of fault current, the transition into MC mode, where the inverter ceases to supply fault current, means that the protective relays fail to detect and

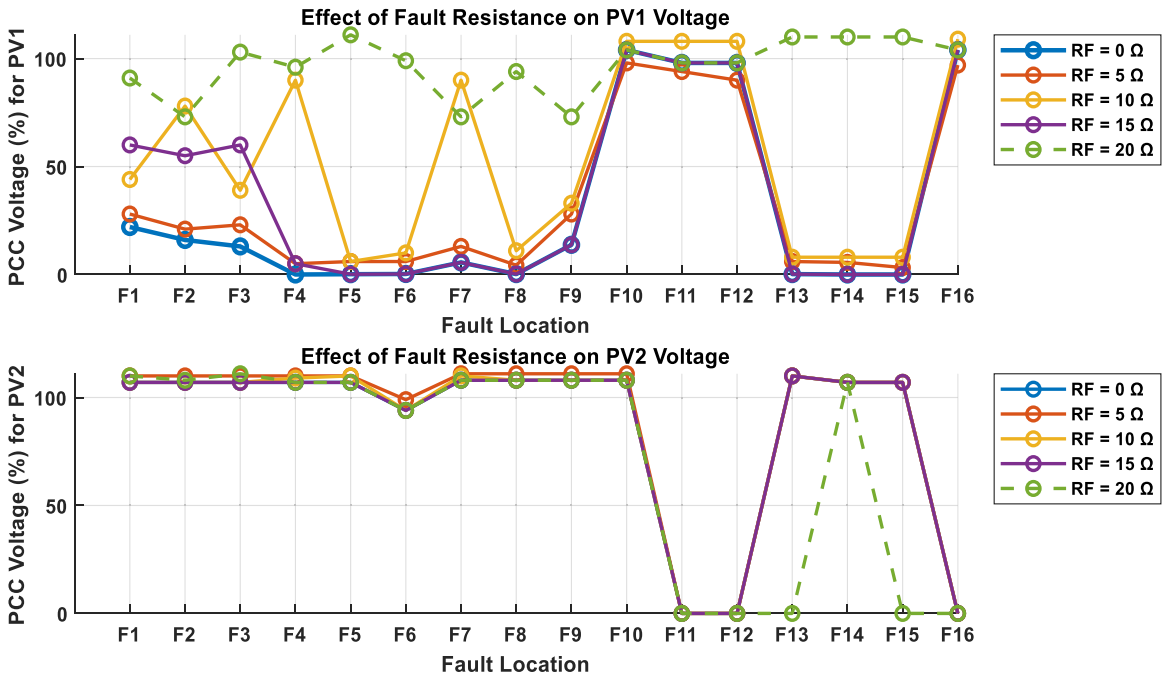

Fig. 22. Effect of FR on MC behaviors.

Table 7
PCC voltage at fault locations for PV1 and PV2 under different fault resistance (Case #3).

Fault	RF=0 ohm		RF=5 ohm		RF=10 ohm		RF=15 ohm		RF=20 ohm	
Location	PV1 Bus 4 (%)	PV2 Bus 13 (%)	PV1 Bus 4 (%)	PV2 Bus 13 (%)	PV1 Bus 4 (%)	PV2 Bus 13 (%)	PV1 Bus 4 (%)	PV2 Bus 13 (%)	PV1 Bus 4 (%)	PV2 Bus 13 (%)
F1	22	107	28	110	44	107	60	107	91	110
F2	16	107	21	110	78	107	55	107	73	108
F3	13	107	23	110	39	107	60	107	103	111
F4	0	107	5	110	90	109	5	107	96	107
F5	0.14	107	6	110	6	110	0.14	107	111	107
F6	0.232	94	6	99	10	94	0.232	94	99	94
F7	5.6	108	13	111	90	110	5.6	108	73	108
F8	0.18	108	4.3	111	11	108	0.18	108	94	108
F9	13.75	108	28	111	33	108	13.75	108	73	108
F10	104	108	98	111	108	108	104	108	104	108
F11	98	0	94	0	108	0	98	0	98	0
F12	98	0	90	0	108	0	98	0	98	0
F13	0.18	110	6	110	8	110	0.18	110	110	0
F14	0	107	5.6	107	8	107	0	107	110	107
F15	0	107	3.2	107	8	107	0	107	110	0
F16	104	0	97	0	109	0	104	0	104	0

respond to the fault. Examining the results, the MC mode depends critically on the voltage level, where the inverter enters cessation if the voltage drops below 0.5 p.u. As indicated in Table 8, the PCC voltage at PV1 fell to as low as 0.2 % at fault F5, and for PV2, it remained at approximately 22 % in most fault scenarios. These voltage drops confirm that the inverter disconnects itself temporarily for around one second before attempting to reconnect. This behavior, while protecting the inverter, effectively isolates the renewable sources, making the over-current protection scheme incapable of detecting faults due to the absence of sufficient fault current. Table 8 shows that at fault locations F11 and F12, the PCC voltage of PV1 rises above 1.1 p.u, causing the inverter to enter the MC mode due to overvoltage shown in Fig. 23. This situation presents a significant problem, as the inverter requires approximately 12 S to reconnect to the network, as illustrated in Fig. 22. This extended duration causes substantial issues in maintaining power supply continuity to the connected loads, leading to instability in the network and making it difficult to effectively utilize the energy sources dependent on this mode. Consequently, the prolonged disconnection undermines the reliability of the system and highlights the challenges of operating under such conditions given this situation, the MC mode offers a layer of protection by halting fault current contribution, but it fundamentally compromises the role of OCRs protection. Without an active fault current, the protection system cannot function as designed, making it impossible to achieve effective fault isolation or selectivity. Overall, operating in island mode with IBRERs demonstrates that traditional OC protection cannot guarantee reliable fault detection when the inverter enters MC mode. The findings, supported by the data showing fault current values consistently at 0.048 A across all fault locations, highlight the inadequacy of relying solely on OC protection in such scenarios. Therefore, a re-evaluation of protection schemes is imperative to ensure system reliability, especially when inverters transition into MC mode under islanding conditions. The results indicate that while the MC mode may maintain coordination in certain scenarios, it introduces substantial risks to grid stability, especially in islanded operations, where a complete loss of power supply occurs.

Table 8
Island mode under MC (Case#4).

Fault Location	Fault Current (A)		Relay Pairs		PCC Voltage	
	Primary (A)	backup (A)	Primary Relay	backup Relay	PV1 Bus 4 %	PV2 Bus 13
F1	0.048	0.048	R1	R2	1	22
F2	0.048	0.048	R2	R3	0.88	18
F3	0.048	0.048	R3	R4	0.6	22
F4	0.048	0.048	R4	R5	0.8	22
F5	0.048	0.048	R5	R6	0.2	23
F6	0.048	0.048	R11	R12	123	0.3
F7	0.048	0.048	R7	R8	0.73	21
F8	0.048	0.048	R8	R9	0.8	20
F9	0.048	0.048	R9	R5	1	22
F10	0.048	0.048	R10	R4	3	22
F11	0.048	0.048	R11	R12	123	0.3
F12	0.048	0.048	R11	R12	123	0.3
F13	0.048	0	DOCR3	DOCR2	0.88	22
F14	0.048	0	DOCR2	DOCR1	1.3	22
F15	0.048	—-	DOCR1	No backup	1	22
F16	0.048	—-	DOCR4	No backup	0	22

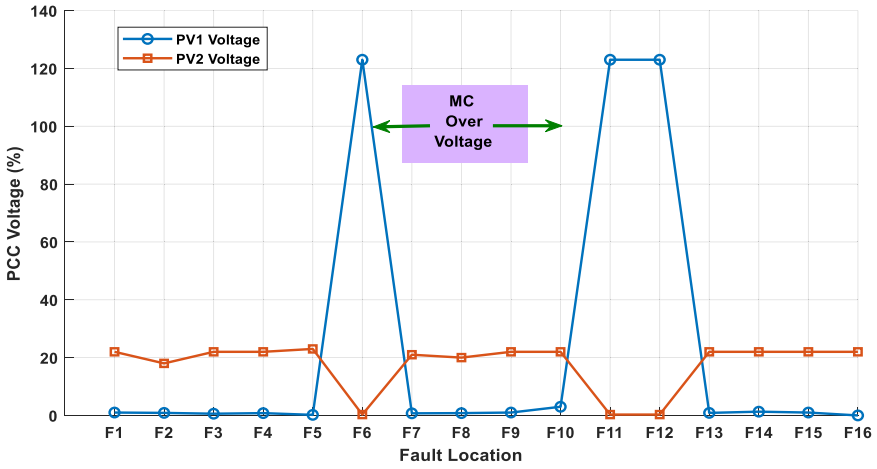

Fig. 23. Voltage profiles during the occurrence of MC under Island mode for all fault conditions (Case#4).

3.2.5. Simulation results of the proposed adaptive OCR scheme

The occurrence of MC during faults presents a significant challenge for OCR, especially in networks with high penetration of inverter-based resources. As highlighted in Section 3.2.3 and demonstrated in Table 6, MC can lead to a complete interruption of the current contribution from the inverter, making conventional OCR ineffective. This is particularly evident in the reverse fault scenarios at fault locations F13, F14, F15, and F16, where the inverter ceases current injection, and as a result, the

Table 9
The performance of the proposed adaptive OCR scheme (VBR) with MC mode.

Fault Location	Fault Current (A)		Relay type		PCC Voltage		Operating time (s)		CTI
	Primary (A)	backup (A)	Primary Relay	backup Relay	PV1 Bus 4 %	PV2 Bus 13 %	Primary (s)	backup (s)	
F1	1251	1251	R1	R2	22	107	0.053	0.3538309	0.3008
F2	1251	1251	R2	R3	16	107	0.346358	0.6438837	0.2975
F3	1378	1378	R3	R4	13	107	0.637974	0.9356278	0.2977
F4	1568	1568	R4	R5	0	107	1.133784	1.4324101	0.2986
F5	2949	2949	R5	R6	0.14	107	1.121471	1.4188877	0.2974
F6	6711	No backup	R6	No backup	0.232	94	1.107	…	1.107
F7	1395	1395	R7	R8	5.6	108	0.050844	0.3481773	0.2973
F8	1474	1474	R8	R9	0.18	108	0.342318	0.6398475	0.2975
F9	1568	0.779	R9	R5	13.75	108	0.32	1.443	1.123
F10	1378	1378	R10	R4	104	108	0.0251	0.641	0.6159
F11	2666	2663	R11	R12	98	0	0.042284	0.3469987	0.3047
F12	6709	No backup	R12	No backup	98	0	0.28	…	0.28
F13	0	0	VBR3	VBR2	0.3	0.3	1.94	2.94	
F14	0	0	VBR2	VBR1	0.18	0.18	0.83	1.37	
F15	0	—-	VBR1	No backup	0.18	107	0.83	No backup	
F16	0	—-	VBR4	No backup	0.18	107	0.83	No backup	

OC protection fails to operate. This issue is further complicated by the inverter's pre-defined reconnection time, during which the relay must decide whether to isolate the inverter from the grid. Therefore, ensuring proper OCR settings is crucial for maintaining reliable fault protection in systems with inverter-based resources. To address this issue, a proposed advanced protection solution (VBR) is introduced by integrating two distinct components. Table 9 and Fig. 24 show that the proposed adaptive solution successfully detected the F13, F14, F15, and F16 with primary tripping time equal to 1.94 S at F13 and 0.83 S for the F14, F15 and F16. Fig. 25 shows the three-phase voltage waveforms under fault F14, with voltage dropping to 0.18 of nominal value for 1 S and the corresponding voltage RMS values.

4. Conclusions and recommendations

The integration of IBRERs, such as solar PV systems, has introduced the phenomenon of MC into power DNs, posing significant challenges to traditional OCR protection schemes. Through simulations conducted using the CIGRE DN model in ETAP and MATLAB, this study investigated four cases to assess the impact of MC on protection coordination. In cases where faults occurred in the radial sections of the network, it was observed that the entry of inverters into MC mode resulted in fault currents being reduced to levels equivalent to the normal operating state, thus maintaining the required coordination between the primary and backup protection relays with a CTI of 0.3 S. This outcome suggests that MC can mimic optimal protection performance in certain configurations. However, in the island mode where the IBRERs act as the primary power source, any occurrence of a fault caused the inverters to enter MC mode due to voltage drops, leading to a complete disconnection of the power supply to all connected loads. This situation eliminated the possibility of selective fault isolation and rendered the traditional OCR protection system ineffective. The study's findings, supported by detailed charts and simulation results, highlight that while MC can assist in maintaining coordination under specific conditions, it presents substantial risks to network stability and protection effectiveness in islanded systems. Moreover, the results demonstrated that fault resistance plays a critical role in determining whether an inverter enters MC. Higher FR tends to keep the inverter in service, preventing unnecessary disconnections. However, this also introduces challenges for the protection system, requiring careful consideration to maintain a balance between reliability and safety. To address these challenges, this study presented an adaptive protection scheme that integrates both current-based and voltage-based logic to improve fault detection and relay performance. The proposed approach ensures rapid, accurate, and adaptive protection under diverse fault scenarios, thereby improving system reliability and operational resilience. Moreover, the coordination between OC protection devices and ESSs (such as batteries) can help mitigate the effects of MC by providing backup power during periods of temporary loss of renewable generation. Finally, updating protection algorithms and employing smart EMS can improve the grid's resilience to sudden changes in generation and load patterns, ensuring faster and more reliable fault detection.

Declarations

All persons who meet authorship criteria are listed as authors, and all authors certify that they have participated sufficiently in the work to take public responsibility for the content, including participation in the concept, design, analysis, writing, or revision of the manuscript. We also confirm that all authors have participated in drafting the article or revising it critically for important intellectual content; and approval of the final version.

Ethical approval

Not applicable.

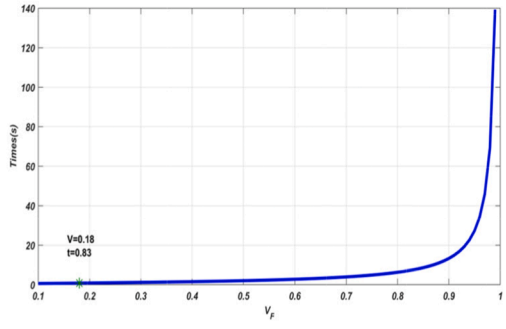

a Response of VBR1and VBR4 under fault F15andF16 (PV)

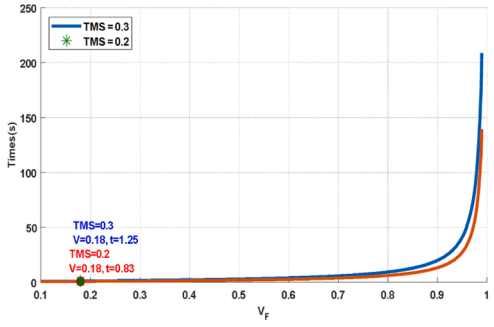

b Response of VBR2 and VBR1 under fault F14

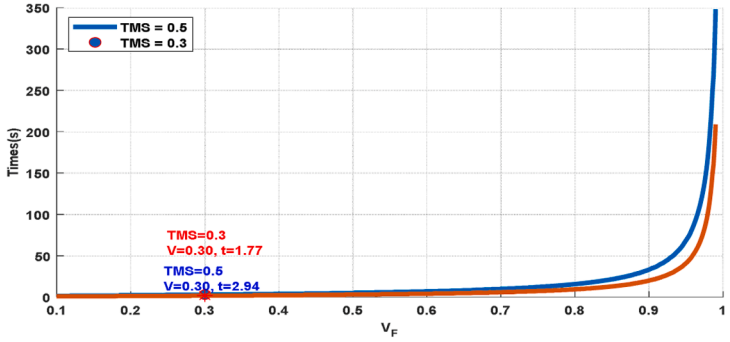

c Response of VBR3 and VBR2 under fault F13.

Fig. 24. Adaptive scheme (VBR) response under fault cases F13, F14, F15 and F16.

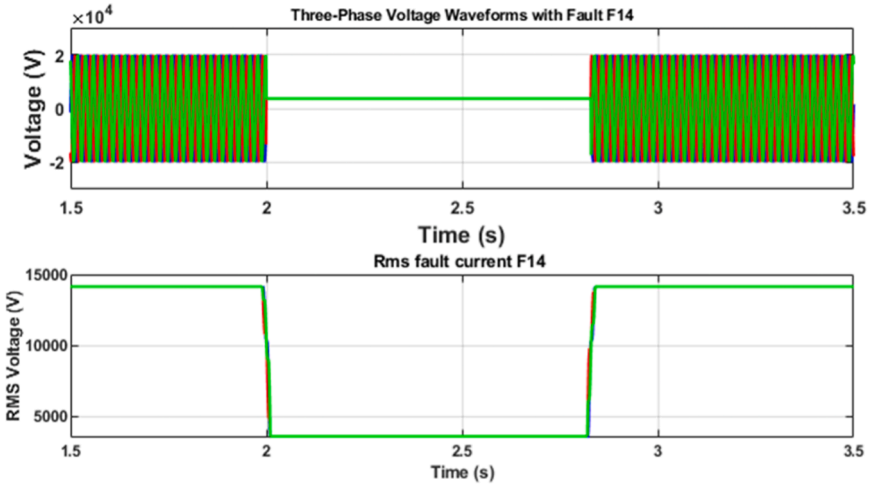

Fig. 25. Three-phase voltage waveforms under fault F14, with voltage dropping to 0.18 of nominal value for 1 S and the corresponding RMS values.

Funding

The authors extend their appreciation to the Deanship of Research and Graduate Studies at King Khalid University for funding this work through Large Research Project under grant number RGP2/238/45.

CRediT authorship contribution statement

Emad Eldeen Omran: Writing – original draft, Software, Methodology, Investigation, Formal analysis, Data curation, Conceptualization. **Feras Alasali:** Writing – review & editing, Writing – original draft, Validation, Supervision, Resources, Methodology, Investigation. **Naser El-Naily:** Writing – original draft, Software, Resources, Methodology, Investigation, Formal analysis, Data curation. **Hassen Loukil:** Writing – review & editing, Validation, Supervision, Software, Project administration, Investigation, Funding acquisition. **Abdelaziz Salah Saidi:** Writing – review & editing, Visualization, Validation, Software, Project administration, Investigation, Conceptualization. **William Holderbaum:** Writing – review & editing, Supervision, Methodology, Formal analysis. **Azza A. ElDesouky:** Writing – review & editing, Visualization, Validation, Supervision, Resources, Project administration, Methodology, Conceptualization.

Declaration of competing interest

We confirm that this work is original and has not been published elsewhere, nor is it currently under consideration for publication elsewhere and the authors declare no conflict of interest. We also confirm that all authors have participated in drafting the article or revising it critically for important intellectual content; approval of the final version.

Acknowledgment

We would like to thank The Hashemite University and University of Salford for their support in publishing this article.

Data availability

Data will be made available on request.

References

[1] M.G. Anany, A.A. ElDesouky, A.A. Salem, Real-time V2G simulator for grid system frequency and voltage regulation with fault ride-through capabilities, Electr. Power Syst. Res. 234 (2024), https://doi.org/10.1016/j.epsr.2024.110561. Sep.

[2] A. ElDesouky, Security constrained generation scheduling for grids incorporating wind, photovoltaic and thermal power, Electr. Power Syst. Res. 116 (1) (2014) 284–292. Nov.

[3] A.A. ElDesouky, E.M. Reyad, G.A. Mahmoud, Implementation of Boolean PSO for service restoration using distribution network reconfiguration simultaneously with distributed energy resources and capacitor banks, Int. J. Renew. Energy Res. 10 (1) (2020) 354–365. Mar.

[4] A.H. Elmetwaly, A.A. ElDesouky, A.A. Sallam, An adaptive D-FACTS for power quality enhancement in an isolated microgrid, IEEE Access 8 (2020) 57923–57942.

[5] S. Eftekharnejad, V. Vittal, G.T. Heydt, B. Keel, J. Loehr, Impact of increased penetration of photovoltaic generation on power systems, IEEE Trans. Power Syst. 28 (2) (2013) 893–901.

[6] D. Khani, A. Sadeghi Yazdankhah, H. Madadi Kojabadi, Impacts of distributed generations on power system transient and voltage stability, Int. J. Electr. Power 43 (1) (2012) 488–500.

[7] C. Li, R. Reinmuller, Fault responses of inverter-based renewable generation: on fault ride-through and Momentary Cessation, in: Proceedings of the IEEE Power and Energy Society General Meeting (PESGM), 2018, pp. 1–5, 5-10 Aug.

[8] S. Zhu, D. Piper, D. Ramasubramanian, R. Quint, A. Isaacs, R. Bauer, Modeling inverter-based resources in stability studies, in: Proceedings of the IEEE Power and Energy Society General Meeting (PESGM), 2018, pp. 1–5, 5-10 Aug.

[9] S. Kang, H. Shin, G. Jang, B. Lee, Impact analysis of recovery ramp rate after Momentary Cessation in inverter-based distributed generators on power system transient stability, IET Gener. Transm. Distrib. (2020).

[10] A. Gargoom, M. Elmusrati, A. Gaouda, Enhancing the operation of smart inverters with PMU and data concentrators, Int. J. Electr. Power Energy Syst. 140 (2022) 108077. September.

[11] H. Shin, B. Lee, K. Iba, Power system regional dependency of distributed energy resources: utilizing the Momentary Cessation capability, IFAC-PapersOnLine 52 (4) (2019) 1–5. Elsevier.

[12] A. Bidram, M.J. Reno, T. Patel, D.J. Kelly, Y. Alkraimeen, Modeling of inverter-based resources for protection studies considering Momentary Cessation, in: Proceedings of the IEEE PES Innovative Smart Grid Technologies Latin America, 2023.

[13] M.N. Alam, B. Das, V. Pant, Protection coordination scheme for directional Overcurrent Relays considering change in network topology and OLTC tap position, Electr. Power Syst. Res. 185 (2020) 106395.

[14] S.A.F. Asl, M. Gandomkar, J. Nikoukar, Optimal protection coordination in the micro-grid including inverter-based distributed generations and energy storage system with considering grid-connected and islanded modes, Electr. Power Syst. Res. 184 (2020) 106317.

[15] M. Usama, M. Moghavvemi, H. Mokhlis, N.N. Mansor, H. Farooq, A. Pourdaryaei, Optimal protection coordination scheme for radial distribution network considering ON/OFF-grid, IEEE Access 9 (2021) 34921–34937. January.

[16] M.H. Sadeghi, A. Dastfan, Y. Damchi, Robust and adaptive coordination approaches for co-optimization of voltage dip and directional Overcurrent Relays coordination, Electr. Power Energy Syst. 129 (2021) 106850.

[17] M.A. Gabr, R.A. El-Sehiemy, T.F. Megahed, Y. Ebihara, S.M. Abdelkader, Optimal settings of multiple inverter-based distributed generation for restoring coordination of DOCRs in mesh distribution networks, Electr. Power Syst. Res. 213 (2022) 108757.

[18] T.D. Firouzabadi, D.A. Zarchi, M. Mazid, H. Safdarkhani, H. Nafisi, Overarching preventive sympathetic tripping approach in active distribution networks without telecommunication platforms and additional protective devices, IEEE Access 10 (2022) 28411–28421. March.

[19] E. Sorrentino, J.V. Rodríguez, Optimal coordination of directional overcurrent protections considering the occurrence probability of different configurations and the effect of grouping cases, Electr. Power Syst. Res. 218 (2023) 109163.

[20] S. Dash, M.K. Jena, P.D. Achlerkar, P. Shaw, Exploring the interdependence between control and protection philosophies in inverter integrated power system: a case study on directional relaying schemes, Electr. Power Syst. Res. 228 (2024) 110074.
[21] IEEE PES Industry Technical Support Task Force, "Impact of IEEE 1547 standard on smart inverters," PES technical report, May. 2018.
[22] F. Alasali, H. Mustafa, A.S. Saidi, N. El-Naily, S. Abeid, W. Holderbaum, S. Saad, The recent development of protection coordination schemes based on inverse of AC microgrid: a review, IET Gener. Transmiss. Distrib. (2023), https://doi.org/10.1049/gtd2.13074.
[23] F. Alasali, H. Albayadrah, N. El-Naily, et al., Highly sensitive protection scheme considering the PV operation control models, Electr. Power Syst. Res. 237 (2024) 111025.
[24] A.A. Ibrahim, A.A. El Desouky, A.A. Salam, Optimal relay setting for utilitydistribution feeders, in: Proceedings of the Twentieth International Middle East Power Systems Conference (MEPCON), 2018.
[25] IEEE Standards Coordinating Committee 21, IEEE Standard for Interconnection and Interoperability of Distributed Energy Resources with Associated Electric Power Systems Interfaces, IEEE, New York, NY, USA, 2018. February.
[26] H. Shin, J. Jung, S. Oh, K. Hur, K. Iba, B. Lee, Evaluating the influence of Momentary Cessation mode in inverter-based distributed generators on power system transient stability, IEEE Trans. Power Syst. 35 (2) (2019) 1618–1626.
[27] A. Chowdhury, K. Nayak, A.K. Pradhan, Positive sequence component based directional relaying for lines integrated with solar photovoltaic plant, Electr. Power Syst. Res. 237 (2024) 111022.
[28] A. Chowdhury, S. Paladhi, A.K. Pradhan, Local positive sequence component based protection of series compensated parallel lines connecting solar photovoltaic plants, Electr. Power Syst. Res. 225 (2023) 109811.
[29] S. Su, Y. Li, X. He, Q. Xie, X. Chen, Z. Zheng, B. Li, J. Zhang, Adaptive current protection for three-phase short-circuits faults in active distribution networks, IET Renew. Power Gener. (2024), https://doi.org/10.1049/rpg2.13170.
[30] Guttromson, R., and Behnke, M., "Momentary Cessation: improving dynamic performance and modeling of utility-scale inverter based resources during grid disturbances", (No. SAND-2020-0266). Sandia National Laboratories (SNL), Albuquerque, NM, and Livermore, CA (United States); Cinch, Inc., Livermore, CA (United States), 2020.
[31] A. Gargoom, M. Elmusrati, A. Gaouda, Enhancing the operation of smart inverters with PMU and data concentrators, Int. J. Electr. Power Energy Syst. 140 (2022) 108077.
[32] M.T. Do, A. Bruyere, B. Francois, Sensitivity analysis of the CIGRE distribution network benchmark according to the large scale connection of renewable energy generators, in: Proceedings of the IEEE Manchester Power Tech, Powertech 2017, 2017, https://doi.org/10.1109/PTC.2017.7981041. Jul.